Abrupt stratospheric vortex weakening associated with North Atlantic anticyclonic wave breaking

Article

Accepted Version

It is advisable to refer to the publisher's version if you intend to cite from the work. See Guidance on citing.

www.reading.ac.uk/centaur

CentAUR

Central Archive at the University of Reading

Reading's research outputs online

Abrupt stratospheric vortex weakening associated with North Atlantic anticyclonic wave breaking

S. H. Lee[1], A. J. Charlton-Perez[1], J. C. Furtado[2], and S. J. Woolnough[3,1]

[1]Department of Meteorology, University of Reading

[2]School of Meteorology, University of Oklahoma

[3]National Centre for Atmospheric Science, University of Reading

Key Points:

- In early February 2018, forecasts abruptly transitioned from indicating a strong stratospheric polar vortex to sudden stratospheric warming.
- This was due to the predictability of a cyclone in the North Atlantic which was associated with driving an anticyclonic Rossby wave break.
- Similar historical cases show this as a mechanism for weakening the stratospheric polar vortex which can lead to major sudden warmings.

Corresponding author: Simon Lee, `s.h.lee@pgr.reading.ac.uk`

Abstract

The sudden stratospheric warming (SSW) of 12 February 2018 was not forecast by any extended-range model beyond 12 days. From early February, all forecast models that comprise the subseasonal-to-seasonal (S2S) database abruptly transitioned from indicating a strong stratospheric polar vortex (SPV) to a high likelihood of a major SSW. We demonstrate that this forecast evolution was associated with the track and intensity of a cyclone in the north-east Atlantic, with an associated anticyclonic Rossby wave break, which was not well-forecast. The wave break played a pivotal role in building the Ural high, which existing literature has shown was a precursor of the 2018 SSW. The track of the cyclone built an anomalously strong sea-level pressure dipole between Scandinavia and Greenland (termed the S-G dipole) which we use as a diagnostic of the wave break. Forecasts which did not capture the magnitude of this event had the largest errors in the SPV strength and did not show enhanced vertical wave activity. A composite of 49 similarly strong wintertime (November–March) S-G dipoles in reanalysis shows associated anticyclonic wave breaking leading to significantly enhanced vertical wave activity and a weakened SPV in the following days, which occured in 35% of the 15-day periods preceding observed major SSWs. Our results indicate a particular transient trigger for weakening the SPV, complementing existing results on the importance of tropospheric blocking for disruptions to the Northern Hemisphere extratropical stratospheric circulation.

Plain Language Summary

During winter, a large circulation 10-50 km above the pole (known as the stratospheric polar vortex) can influence the day-to-day weather patterns in the troposphere beneath from weeks to months later. Thus, being able to predict the behavior of the stratospheric polar vortex is important for predicting the weather on longer time-frames. In February 2018, the Northern Hemisphere stratospheric polar vortex broke apart in an event known as a sudden stratospheric warming, which was not well-forecast. This event led to unusually cold conditions across Eurasia. In this article we find the poor predictability of the event was due to a poorly forecast weather system in the Atlantic. We also show that this pattern was present in previously observed cases where the stratospheric polar vortex has weakened. Our results demonstrate a trigger mechanism for these extreme events and have implications for our ability to predict the weather at longer ranges.

1 Introduction

The major mid-winter sudden stratospheric warming (SSW) event of 12 February 2018 was the first major SSW since January 2013 (defined as a reversal of the daily-mean 10 hPa 60°N zonal-mean zonal winds (Charlton & Polvani, 2007)), a 5 year gap which was the longest since 1989–1998 according to the SSW Compendium (Butler, Sjoberg, Seidel, & Rosenlof, 2017). It produced a split of the stratospheric polar vortex (SPV) into two smaller vortices. Following the metric of Karpechko, Hitchcock, Peters, and Schneidereit (2017) the event was downward-propagating with the negative phase of the stratospheric Northern Annular Mode (NAM) (Baldwin & Dunkerton, 2001; Thompson & Wallace, 2000) accompanied by a strong and persistent negative tropospheric NAM in the 45 days following the event. The negative tropospheric NAM and associated negative North Atlantic Oscillation (NAO) produced extremely cold conditions across Europe and northern Asia, with a large anticyclone over Scandinavia generating a cold easterly flow (Ferranti, Magnusson, Vitart, & Richardson, 2018). With such a high impact response, the ability to predict the onset of an SSW like in 2018 is of vital importance for sub-seasonal forecasting.

The 2018 SSW was the first to occur following the development of the subseasonal-to-seasonal (S2S) database of extended-range forecasts from 11 international forecast models (Vitart et al., 2017). None of the S2S model forecasts issued at the time indicated a major SSW until early February (Karpechko, Charlton-Perez, Balmaseda, & Vitart, 2018), giving a predictability window less than the medium-range timeframe (∼2 weeks). Although this lies within the window typical of predicting major SSWs (Taguchi, 2014; Tripathi et al., 2016, 2015), S2S model forecasts abruptly transitioned from projecting a strong SPV to a weak SPV/major SSW in late January-early February, with a corresponding transition in forecasts of tropospheric conditions (such as from forecasts of a positive NAO to a negative NAO). Karpechko (2018) showed several SSWs were poorly forecast in ECMWF hindcasts at lead-times beyond 7–10 days, but most were generally associated with a longer-range signal of SSW likelihood.

Specifically for the February 2018 event, Karpechko et al. (2018) examined S2S model forecasts from 1 February onwards and showed a strong relationship between the accuracy of stratospheric wind forecasts and the intensity of an anticyclone over the Urals (named the 'Ural high'). However, they did not assess the longer-term predictability of

⁷⁷ the event, the mechanism driving the onset of the Ural high, or its influence on the strato-

⁷⁸ sphere, leaving open questions about the abrupt predictability onset. The Ural high has

⁷⁹ also been shown to drive SPV variability (Peings, 2019; White et al., 2019) by project-

⁸⁰ ing onto the climatological stationary wave pattern.

⁸¹ Most studies of SSW precursors use a 'top-down' perspective, where the tropospheric

⁸² features are analyzed in the period preceding observed stratospheric events. These ap-

⁸³ proaches typically discern stationary or longer-lived features through the process of av-

⁸⁴ eraging anomalies in the build-up to SSWs. Tropospheric blocking is one such feature

⁸⁵ (e.g. Colucci & Kelleher, 2015; Garfinkel, Hartmann, & Sassi, 2010; Julian & Labitzke,

⁸⁶ 1965; Martius, Polvani, & Davies, 2009; Quiroz, 1986). For example, Bao, Tan, Hart-

⁸⁷ mann, and Ceppi (2017) used cluster analysis to assess 500 hPa geopotential height pat-

⁸⁸ terns in the month before 37 SSWs in reanalysis, and found the patterns to be associ-

⁸⁹ ated with linear interference with climatological stationary waves. Kolstad and Charlton-

⁹⁰ Perez (2011) used reanalysis alongside climate model simulations and found a particu-

⁹¹ larly strong signal for a height anomaly dipole over northern Eurasia preceding 'weak

⁹² vortex months'. Other studies have considered more transient features associated with

⁹³ specific stratospheric events. Coy, Eckermann, and Hoppel (2009) noted the importance

⁹⁴ of zonal wavenumbers 4-5 associated with synoptic-scale systems preceding the SSWs

⁹⁵ of January 2006 and 2003. They implicated tropospheric systems over the North Atlantic

⁹⁶ and subtropical wave breaking; forecasting experiments showed a realistic SSW only oc-

⁹⁷ curred when a North Atlantic weather system was correctly represented in the model.

⁹⁸ On the other hand, a study of the January 2013 SSW (Coy & Pawson, 2014) suggested

⁹⁹ a rapidly-deepening cyclone in the North Atlantic played only a minor role, acting as a

¹⁰⁰ transient source of vertical wave activity that was not crucial to forcing the event. The

¹⁰¹ authors also remark on the dynamical link between the initial stratospheric vortex state

¹⁰² and the track of the cyclone, suggesting a two-way relationship. O'Neill, Oatley, Charlton-

¹⁰³ Perez, Mitchell, and Jung (2017) demonstrated a link between extratropical tropospheric

¹⁰⁴ cyclogenesis occurring at the edge of the SPV and split-type SSWs through a potential

¹⁰⁵ vorticity framework. Although mainly focusing on the Southern Hemisphere SSW of 2002

¹⁰⁶ (e.g. Krüger, Naujokat, & Labitzke, 2005), they briefly show a similar mechanism with

¹⁰⁷ cyclogenesis over the eastern seaboards of the Northern Hemisphere continents. Most

¹⁰⁸ recently, Attard and Lang (2019) approach the problem by looking at the meridional eddy

¹⁰⁹ heat flux, and demonstrate the different responses for blocks and 'bomb' cyclones in the

110   Atlantic and Pacific sectors. They conclude cold-season Atlantic bomb cyclones and Pa-

111   cific blocks were associated with negative heat flux anomalies (and vice versa) whilst also

112   noting that only a relatively small number of blocks and bombs are actively associated

113   with SSWs.

114   Thus, there exist both transient and stationary drivers of stratospheric variabil-

115   ity (including but not limited to SSWs), the predictability of which plays a role in the

116   onset of SSW prediction. In this study, we provide a dynamical explanation for the abrupt

117   transition in the forecasts of the February 2018 event, building upon existing analysis.

118   We demonstrate that this is a characteristic of historical cases of vortex weakening, rather

119   than unique to the flow configuration driving the 2018 event, through a 'bottom-up' ap-

120   proach (analysing the response of the stratosphere to tropospheric events). Our results

121   have implications for extended-range predictability of SSWs and thus sub-seasonal tro-

122   pospheric forecasts.

2 Data and Methods

124   We use forecast data from the European Centre for Medium Range Weather Fore-

125   casts (ECMWF) and National Centers for Environmental Prediction (NCEP) models,

126   as these provide a combination of both large ensemble sizes and frequent launch dates

127   - ECMWF launches twice weekly (Tuesday and Thursday) with 51 members, and NCEP

128   launches daily with 16 members. The predictability onset of the SSW was common across

129   all the S2S models (Karpechko et al., 2018), so our analysis is not sensitive to the choice

130   of model. For verification, we use the ECMWF ERA-Interim reanalysis (Dee et al., 2011).

131   The strength of the SPV is defined using the zonal-mean zonal wind at 10 hPa and 60°N

132   ($U10_{60}$). We use 45–75°N meridionally-averaged zonal-mean eddy heat flux (denoted as

133   [v*T*] where the star notation indicates a departure from the zonal-mean, and square

134   brackets indicate a zonally-averaged quantity) at 300 hPa as a proxy for upper-tropospheric

135   wave activity. This is proportional to the vertical component of the Eliassen-Palm flux

136   (Andrews, Holton, & Leovy, 1987). Standardized polar cap (60–90°N) geopotential height

137   anomalies are used as a proxy for the NAM index (Karpechko et al., 2017); the anoma-

138   lies are inversely proportional to the index. Unless otherwise stated, standardized anoma-

139   lies are computed with respect to the climatological daily-mean and standard deviation

140   in ERA-Interim. Historical composites use data from January 1979–March 2017 inclu-

141   sive, and statistical significance is assessed using a bootstrap re-sampling method with

replacement ($n = 50{,}000$) for November–March in the period January 1979 to March 2017. Potential vorticity is analyzed on the 315 K isentropic surface in ERA-Interim data and the 320 K isentropic surface in model forecast data as these are the nearest tropospheric levels available in both datasets. All data are re-gridded to 2.5° horizontal resolution for consistency.

3 Results

3.1 Characterizing the Onset of SSW Predictability

To demonstrate the evolution of forecasts of the zonal-mean state, Figure 1 (a, c) shows forecasts of $U10_{60}$ for the first 5 days of the verifying SSW (12–16 February) for all forecasts in which those dates featured. There is an abrupt transition in late January-early February from forecasts of a strong vortex to a weakened vortex or major SSW. In both ECMWF and NCEP systems, the 29 January ensembles showed no members indicating mean easterlies during this period, with a tightly clustered ensemble. The following day, forecasts from NCEP substantially changed, with some members suggesting a mean zonal wind reversal and the entire ensemble forecasting weaker $U10_{60}$ than the 25th percentile of the ensemble from the previous day – a change which also occurred in the 29 January and 1 February ECMWF ensembles. There is also an increase in spread despite the reduced lead-time. Ensemble spread was then much reduced by 5-6 February, a lead-time of only 6-7 days before the major SSW. A similar predictability evolution is found in other S2S models (not shown), indicating this was not related to the ability of certain models to capture the event. Moreover, we see the abrupt transition of vortex strength was associated with an abrupt increase in 300 hPa [v*T*] preceding the wind reversal (Figure 1b and 1d). The increase in forecast heat flux suggests the low predictability of the SSW was dependent on poorly-forecast tropospheric wave-driving, rather than the response of the stratospheric vortex to a wave pulse or the sensitivity of the $U10_{60}$ metric.

To investigate this evolution further, we look at the 29 January and 1 February ensembles from ECMWF, which cover the spread of evolutions from strong vortex to weak vortex (Figure 2). The ensembles systematically diverge after 5 February – with the forecasts from 29 January showing low wave activity and strengthening zonal-mean zonal winds, whilst the opposite is true for forecasts from 1 February. This is an even greater

173   divergence in zonal wind intensity than day-15 forecasts for the January 2013 SSW shown

174   in Tripathi et al. (2016). Despite the 3 day difference in lead-time, the systematic dif-

175   ference between the two ensembles motivates considering them together to capture the

176   uncertainty. Analysis in the corresponding NCEP ensembles gives similar results (see Fig-

177   ure S1).

178   Thus, there are two alternative scenarios demonstrated in ensemble forecasts from

179   late January and early February: (a) enhanced vertical wave activity around 5 Febru-

180   ary leading to SPV weakening, and (b) suppressed wave activity with little subsequent

181   change in SPV strength. In the next section, we discern the tropospheric drivers for these

182   divergent stratospheric evolutions.

183   **3.2 Characterizing Tropospheric Uncertainty**

184   Figure 3 depicts the linear correlation between the mean $U10_{60}$ forecast for 9–11

185   February (a period where ensemble members either projected a quiescent vortex or strong

186   deceleration, c.f. Figure 2) and the mean sea-level pressure (MSLP) for 3–5 February (i.e.,

187   just before the onset of enhanced vertical wave flux). This correlation is calculated in

188   joined ensembles from 29 January to 1 February in NCEP (to increase ensemble sam-

189   ple size and incorporate a larger range of SPV strengths), and 29 January and 1 Febru-

190   ary in ECMWF; independent calculations (not shown) for the separate ensembles sug-

191   gest this is not a result of the difference in character of the forecasts or a facet of the dif-

192   ferences in lead-time. We average across forecasts initialized during the onset of predictabil-

193   ity of the vortex weakening event (c.f. Figure 1) to determine what changed during this

194   window. The results show the strongest correlations between the preceding MSLP field

195   and the strength of the SPV form a dipole between Scandinavia and Greenland. Secondary

196   regions of strong correlation are also located upstream and downstream of the main dipole.

197   The correlation field indicates that ensemble members with lower MSLP over eastern Green-

198   land and higher MSLP over Scandinavia forecast weaker $U10_{60}$. Based on this correla-

199   tion analysis, we define the Scandinavia-Greenland dipole in MSLP (hereafter, the S-G

200   dipole) to describe the evolution. We calculate this by subtracting the area-average MSLP

201   in a grid box over Scandinavia (60-70°N, 12.5-42.5°E) from that in a grid box over east-

202   ern Greenland (72.5-90°N, 2.5-42.5°W). The MSLP in each grid box is cosine-weighted

203   to account for the convergence of meridians at higher latitudes. The two nodes, primar-

204   ily based on the track of a cyclone and the development of a Scandinavian ridge (see Fig-

205   ure 4), are shown as black dashed lines in Figure 3. The Ural high, also shown Figure

206   3, is defined as the area-average MSLP in the grid box 45-60°N, 50-80°E.

207   To discern the tropospheric drivers of the vertical wave flux, we assess the MSLP

208   evolutions of ECMWF ensemble members from 29 January and 1 February 2018 with

209   the top and bottom 10%-mean 300 hPa [v*T*] for 4–6 February. Results (Figure 4) sup-

210   port the correlation analysis from Figure 3; a cyclone near Iceland on 3 February pro-

211   gresses up the eastern coast of Greenland and deepens to <970 hPa by 5 February in

212   the high-flux members, with a ridge extending from the Azores through Scandinavia, whilst

213   in the low-flux members the cyclone moves south-east towards Europe and weakens with-

214   out any ridge development. Figure 4c demonstrates the dipole structure; pressures are

215   >20 hPa higher (lower) over Scandinavia (Greenland) in the top 10% versus the bottom

216   10% heat flux members. A similar result is found when the same analysis is performed

217   in the NCEP forecasts (see Figure S2).

218   Next we compare the evolution of the S-G dipole with that of the Ural high (af-

219   ter Karpechko et al. (2018)) (Figure 5). The S-G dipole peaked at 52 hPa in ERA-Interim

220   on 5 February. There is rapid divergence after 3 February in accordance with Figure 4

221   (due to discrepancies in both nodes of the dipole), whilst it is also shown that the en-

222   semble members with the largest heat flux more closely follow ERA-Interim verification.

223   There is also a lagged relationship between the S-G dipole evolution and the Ural high,

224   and ensemble members with lowest mean 300 hPa heat flux lack both a strong S-G dipole

225   and Ural high. Inspecting potential vorticity (PV) on the 320 K isentropic surface in en-

226   semble members with the top 10% mean 300 hPa heat flux (Figure 6a) shows a tongue

227   of low PV air (<2 PVU) protruding polewards in the Atlantic sector east of Greenland

228   on 5 February before becoming cut-off and overturning on 8 February, indicative of an

229   anticyclonic Rossby wave break. This evolution is spatially and temporally coherent with

230   both the cyclone track/S-G dipole development and the 300 hPa heat flux. The wave

231   break is not present in ensemble members with the lowest 10% heat flux, which corre-

232   spondingly lacked a strong S-G dipole (Figure 6b). Thus, the predictability of the wave

233   breaking event and its impact on the stationary wave pattern indicates a possible expla-

234   nation for the abrupt forecast transition, as well as a dynamical mechanism by which

235   the S-G dipole in MSLP relates to both enhanced wave activity and amplification of the

236   Ural high downstream (through the attendant upper-level PV anomaly).

237 The relationship between the S-G dipole, the Ural high, and 300 hPa heat flux in

238 February 2018 is shown in Figure 7. Forecast heat flux increases approximately linearly

239 with S-G dipole strength ($r = 0.79$ in NCEP vs. 0.75 in ECMWF) and heat flux is only

240 enhanced for values of the S-G dipole above ∼40 hPa. However, not all ensemble mem-

241 bers with an enhanced dipole produce enhanced heat flux; members with the strongest

242 heat flux feature both an amplified S-G dipole *and* a strengthened Ural high. Thus, the

243 enhancement of wave activity and amplification of the Ural high was dependent upon

244 the prior occurrence of the S-G dipole/wave breaking event as well as specifics of the wave

245 break and its interaction with the stratosphere. Figure 8 illustrates the surface evolu-

246 tion of the Ural high over 6–8 February in high vs. low heat flux members (c.f. Figure

247 4 and Figure S3). The anticyclone that develops over the Urals on 8 February in the high

248 heat flux members is the same system that is present over Scandinavia in the preced-

249 ing days associated with one node of the S-G dipole; this anticyclone is absent in the low

250 heat flux members, and thus directly links the evolution of the Ural high to the S-G dipole.

251 Therefore, the two precursors are not independent.

252 **3.3 Historical S-G Dipoles**

253 In this section we consider historical cases in extended-winter (November–March)

254 where the S-G dipole exceeds 40 hPa (similar in magnitude to the 2018 event, and ap-

255 proximately equal to the 99th percentile of daily November–March 1979-2017 ERA-Interim

256 climatology) to discern whether the dipole is a characteristic of previous cases of SPV

257 weakening. This threshold is not influenced by the time of year of an individual event,

258 as there is little day-to-day variability in the daily-mean and standard deviation of the

259 S-G dipole through the extended winter period. The Ural high is also considered, and

260 by using these previous examples we seek to understand whether the dipole or the Ural

261 high was the root cause of the enhanced vertical wave activity.

262 Motivated by Charlton and Polvani (2007) and their consideration of stratospheric

263 radiative timescales, we use a window of 20 days to separate individual events, yielding

264 a total of 49 cases (listed in Table S1). The strongest S-G dipole, 56 hPa, occurred on

265 15 March 2015. In Figure 9 we see the MSLP lag-composite anomaly evolution, with a

266 cyclone tracking up eastern Greenland into the Arctic region and a concomitant anti-

267 cyclone over Scandinavia. Notably the anticyclone is of greater persistence throughout

268 this period with transient amplification upon the passage of the cyclone. Following the

269 dipole peak, the anomaly field resembles the Scandinavian blocking Atlantic weather regime

270 (Cassou, Terray, Hurrell, & Deser, 2004; Charlton-Perez, Ferranti, & Lee, 2018) and is

271 similar to the precursors to weak SPV episodes shown in Kolstad and Charlton-Perez

272 (2011).

273 These historical events are also associated with anticyclonic wave breaking (Fig-

274 ure 10) similar to that which occurred in 2018, with the wave break in the Atlantic and

275 northern Europe evident through the reversal of the meridional PV gradient on the 315

276 K isentropic surface in this region. Composites of 45–75°N [v*T*] and 60–90°N geopo-

277 tential height for 30 days before and after the peak of the dipole are shown in Figure 11.

278 Strong S-G dipoles are associated with a significant vertical wave pulse, and a weaken-

279 ing of the SPV (increasing polar cap geopotential heights indicating a negative strato-

280 spheric NAM tendency) in 10–15 days. It should be emphasized that these results show

281 relative vortex weakening, rather than the development of a climatologically weak vor-

282 tex. Indeed, some cases show a weakening of a strong SPV, or a temporary reduction

283 in the rate of vortex intensification, following an S-G dipole event. The evolution in 2018

284 (not shown) is very similar to the composites, albeit with increased magnitude.

285 To discern whether these historically strong S-G dipoles were also associated with

286 enhanced Ural highs, we analyse the change in the Ural high at a 3-day lag from the dipole

287 peak (motivated by the evolution in 2018). There is no clear tendency toward either a

288 strengthening or a weakening Ural high ($\mu = 0.3$ hPa, $\sigma = 10.3$ hPa). Splitting the com-

289 posites by whether the Ural high weakens or strengthens does not significantly alter the

290 composites: strong S-G dipoles followed by a weakening of the Ural high still show en-

291 hanced heat flux and a weakened polar vortex in the following days. This indicates it

292 is the wave break associated with the S-G dipole, not the resultant Ural high, which drives

293 the enhanced vertical wave flux - and that instead, in 2018, the Ural high was a conse-

294 quence of the preceding evolution.

295 Next, we assess the association between the S-G dipole and observed major mid-

296 winter SSWs prior to 2018 (Table 1). Of the 23 SSWs (Karpechko et al., 2017), we find

297 8 (35%) followed a similar evolution to 2018 and were preceded by an S-G dipole exceed-

298 ing 40 hPa within 15 days of the start date of the SSW. Given the total of 345 days pre-

299 ceding the 23 events (and assuming independence), this is 2.3 times larger than the cli-

300 matological likelihood (since 40 hPa is approximately the 99th percentile, it would be

301   expected that it was exceeded on 3-4 days). We note that the 2018 event was stronger

302   than any of these prior events associated with major SSWs (the previous strongest be-

303   ing 48 hPa preceding the major SSW in March 1981), possibly a facet of 2018 being the

304   event used to define the index. Although the major SSW in February 2018 was a vor-

305   tex split, 6 of the observed SSWs with a strong S-G dipole precursor were displacement

306   events (Karpechko et al., 2017) suggesting this pattern does not itself induce a specific

307   stratospheric evolution but acts to amplify an existing planetary wave structure. When

308   2018 is included, 78% of the major SSWs preceded by an amplified S-G dipole were downward-

309   propagating (Karpechko et al., 2017), with only March 1981 and February 2008 other-

310   wise. This is larger than the observed ratio of 57% (although the sample is too small to

311   draw robust conclusions), but is in agreement with Birner and Albers (2017) who note

312   larger tropospheric impacts following SSWs preceded by enhanced tropospheric wave ac-

313   tivity. We further note that 33% (90%) of the S-G dipole events considered here were

314   associated with daily 500 hPa [v*T*] exceeding 2 σ (1 σ) within 5 days either side of the

315   events, indicating the dipole is an important contributor to anomalously high zonal-mean

316   tropospheric wave flux in general.

4 Discussion and Conclusions

318   In this study we have shown that the abrupt onset of predictions of stratospheric

319   polar vortex (SPV) weakening and sudden stratospheric warming (SSW) in February 2018

320   was driven by an anticyclonic Rossby wave break (Figure 6) associated with the track

321   and intensity of a cyclone over eastern Greenland, and an associated ridge over Scan-

322   dinavia. From this, we define a Scandinavia-Greenland (S-G) dipole index in MSLP to

323   describe the evolution, and show that this was not well-forecast at long lead-times. The

324   location and intensity of the cyclone was a rare occurrence, with the mean MSLP in the

325   Greenland node and the dipole itself exceeding the 99th percentile of extended winter

326   months from 1979-2017. Occurrences of similarly strong S-G dipoles in reanalysis are shown

327   to be associated with anticyclonic wave breaking in the Atlantic sector (Figure 10), which

328   induces anomalously strong vertical wave activity (Figure 11a), and a rapid tendency

329   towards a weakened SPV/negative stratospheric NAM (Figure 11b) within 10 days. This

330   indicates that the evolution in 2018 was not a characteristic of the specific flow config-

331   uration but a more general mechanism for vortex weakening present in other events.

We have also shown that the S-G dipole and wave breaking event was important for amplifying a high pressure system over the Urals, first described in Karpechko et al. (2018) as a surface-pressure precursor of the 2018 SSW. Our results suggest that the Ural high was likely a consequence of the wave breaking event which drove stratospheric wave activity leading to the SSW, rather than a primary driver itself. The initial divergence in the evolution of the SPV strength and the onset of the enhanced vertical wave flux occurred around 5 February (Figure 2), preceding the amplification of the Ural high which followed on 8 February (Figure 5b), which further indicates the Ural high was a secondary response. It is likely that the persistence of the Ural high might have resulted in its detection in the averaging used in Karpechko et al. (2018), rather than the transience of the S-G dipole/wave break.

Our results differ from previous work through using a 'bottom-up' perspective, assessing the stratospheric response to tropospheric events. We provide a particular *transient* trigger which would not be easily distinguished through 'top-down' time-mean composites (where the tropospheric configuration prior to stratospheric events is considered). This helps illuminate mechanisms by which persistent tropospheric blocking, including Scandinavian blocking which has previously been shown to precede SSWs (Cohen & Jones, 2011; Kolstad & Charlton-Perez, 2011; Martius et al., 2009), can produce *sudden* changes in the stratospheric circulation. Furthermore, our results apply to a wider range of SPV variability than major SSWs – even the case of weakening a climatologically strong vortex towards an average state – which helps describe precursors of a larger proportion of the sub-seasonal behaviour. We therefore suggest the S-G dipole should be monitored operationally as a precursor to SPV weakening. Changes and uncertainty in its forecasts may help to qualitatively identify sources of uncertainty in stratospheric forecasts.

The intensity of the S-G dipole in 2018 was not well-forecast, driven by uncertainty in the track and intensity of an Atlantic cyclone. At longer lead-times, model biases in storm track and intensity may negatively impact the skill in predicting such events. For example, Frame, Methven, Roberts, and Titley (2015) showed cyclone intensity decayed with lead-time up to 15 days, which would constrain the ability of forecast models to produce strong S-G dipoles sufficient for strong wave breaking and vortex weakening, whilst Gray, Dunning, Methven, Masato, and Chagnon (2014) and Saffin, Gray, Methven, and Williams (2017) also showed biases in tropopause PV and Rossby wave structure which may limit the ability to capture these types of wave breaking episodes and associated

stratospheric variability. These considerations are consistent with a deterministic limit on SSW predictability (Karpechko, 2018; Taguchi, 2018).

The occurrence of strong S-G dipoles requires a poleward-shifted Atlantic storm track, which is associated with the positive NAM/NAO pattern. This is often related to the prior occurrence of a strengthened SPV (e.g. Baldwin & Dunkerton, 2001) and SSWs are typically preceded by strong SPV conditions (e.g. Charlton & Polvani, 2007). This behaviour could imply a two-way coupling in which the vortex drives its own variability - akin to a self-sustaining oscillator. Several studies (e.g. Lorenz & DeWeaver, 2007; Tamarin & Kaspi, 2017) have indicated a poleward shift in the North Atlantic storm track during winter under future climate change. This may lead to an increased frequency of strong S-G dipoles and thus more frequent wave breaking events and stratospheric vortex weakening, but the aforementioned biases may reduce the ability of climate models to fully represent this source of sub-seasonal variability.

Acknowledgments

References

Andrews, D., Holton, J., & Leovy, C. (1987). *Middle Atmosphere Dynamics.* Academic Press.

Attard, H. E., & Lang, A. L. (2019). Troposphere-stratosphere coupling following tropospheric blocking and extratropical cyclones. *Monthly Weather Review*, MWR–D–18–0335.1. doi: 10.1175/MWR-D-18-0335.1

Baldwin, M. P., & Dunkerton, T. J. (2001). Stratospheric harbingers of anomalous

weather regimes. *Science*, *294*(5542), 581–584. doi: 10.1126/science.1063315

Bao, M., Tan, X., Hartmann, D. L., & Ceppi, P. (2017). Classifying the tropospheric precursor patterns of sudden stratospheric warmings. *Geophysical Research Letters*, *44*(15), 8011–8016. doi: 10.1002/2017GL074611

Birner, T., & Albers, J. R. (2017). Sudden stratospheric warmings and anomalous upward wave activity flux. *Sola*, *13A*(Special_Edition), 8–12. doi: 10.2151/sola .13a-002

Butler, A. H., Sjoberg, J. P., Seidel, D. J., & Rosenlof, K. H. (2017). A sudden stratospheric warming compendium. *Earth System Science Data*, *9*(1), 63–76. doi: 10.5194/essd-9-63-2017

Cassou, C., Terray, L., Hurrell, J. W., & Deser, C. (2004). North Atlantic winter climate regimes: spatial asymmetry, stationarity with time, and oceanic forcing. *Journal of Climate*, *17*(5), 1055–1068. doi: 10.1175/1520-0442(2004)017⟨1055: NAWCRS⟩2.0.CO;2

Charlton, A. J., & Polvani, L. M. (2007). A new look at stratospheric sudden warmings. part i: climatology and modelling benchmarks. *J. Climate*, *20*(3), 449-469. doi: 10.1175/JCLI3996.1

Charlton-Perez, A. J., Ferranti, L., & Lee, R. W. (2018). The influence of the stratospheric state on North Atlantic weather regimes. *Quarterly Journal of the Royal Meteorological Society*, *144*(713), 1140–1151. doi: 10.1002/qj.3280

Cohen, J., & Jones, J. (2011). Tropospheric precursors and stratospheric warmings. *Journal of Climate*, *25*(5), 1780–1790. doi: 10.1175/JCLI-D-11-00701.1

Colucci, S. J., & Kelleher, M. E. (2015). Diagnostic comparison of tropospheric blocking events with and without sudden stratospheric warming. *Journal of the Atmospheric Sciences*, *72*(6), 2227–2240. doi: 10.1175/jas-d-14-0160.1

Coy, L., Eckermann, S., & Hoppel, K. (2009). Planetary wave breaking and tropospheric forcing as seen in the stratospheric sudden warming of 2006. *Journal of the Atmospheric Sciences*, *66*(2), 495–507. doi: 10.1175/2008jas2784.1

Coy, L., & Pawson, S. (2014). The major stratospheric sudden warming of January 2013: analyses and forecasts in the GEOS-5 data assimilation system. *Monthly Weather Review*, *143*(2), 491–510. doi: 10.1175/mwr-d-14-00023.1

Dee, D. P., Uppala, S. M., Simmons, A. J., Berrisford, P., Poli, P., Kobayashi, S., . . . Vitart, F. (2011). The ERA-Interim reanalysis: configuration and performance

429 of the data assimilation system. *Quarterly Journal of the Royal Meteorological*
430 *Society*, *137*(656), 553–597. doi: 10.1002/qj.828

431 Ferranti, L., Magnusson, L., Vitart, F., & Richardson, D. (2018). A new prod-
432 uct to flag up the risk of cold spells in Europe weeks ahead. *ECMWF Newslet-*
433 *ter*(158), 1–8. doi: 10.21957/k2rlf88oe1

434 Frame, T. H. A., Methven, J., Roberts, N. M., & Titley, H. A. (2015). Predictability
435 of frontal waves and cyclones. *Weather and Forecasting*, *30*(5), 1291–1302. doi:
436 10.1175/waf-d-15-0039.1

437 Garfinkel, C. I., Hartmann, D. L., & Sassi, F. (2010). Tropospheric precursors
438 of anomalous northern hemisphere stratospheric polar vortices. *Journal of*
439 *Climate*, *23*(12), 3282–3299. doi: 10.1175/2010JCLI3010.1

440 Gray, S. L., Dunning, C. M., Methven, J., Masato, G., & Chagnon, J. M. (2014).
441 Systematic model forecast error in Rossby wave structure. *Geophysical Re-*
442 *search Letters*, *41*(8), 2979–2987. doi: 10.1002/2014GL059282

443 Julian, P. R., & Labitzke, K. B. (1965). A study of atmospheric energetics during
444 the January–February 1963 stratospheric warming. *Journal of the Atmospheric*
445 *Sciences*, *22*(6), 597–610. doi: 10.1175/1520-0469(1965)022⟨0597:asoaed⟩2.0.co;
446 2

447 Karpechko, A. Y. (2018). Predictability of sudden stratospheric warmings in the
448 ECMWF extended-range forecast system. *Monthly Weather Review*, *146*(4),
449 1063–1075. doi: 10.1175/MWR-D-17-0317.1

450 Karpechko, A. Y., Charlton-Perez, A., Balmaseda, T. N., Magdalena, & Vitart,
451 F. (2018). Predicting sudden stratospheric warming 2018 and its climate
452 impacts with a multimodel ensemble. *Geophysical Research Letters*, *45*(24),
453 13,538–13,546. doi: 10.1029/2018GL081091

454 Karpechko, A. Y., Hitchcock, P., Peters, D. H. W., & Schneidereit, A. (2017). Pre-
455 dictability of downward propagation of major sudden stratospheric warmings.
456 *Quarterly Journal of the Royal Meteorological Society*, *143*(704), 1459–1470.
457 doi: 10.1002/qj.3017

458 Kolstad, E. W., & Charlton-Perez, A. J. (2011). Observed and simulated precur-
459 sors of stratospheric polar vortex anomalies in the Northern Hemisphere. *Cli-*
460 *mate Dynamics*, *37*(7-8), 1443–1456. doi: 10.1007/s00382-010-0919-7

461 Krüger, K., Naujokat, B., & Labitzke, K. (2005). The unusual midwinter warming in

the Southern Hemisphere stratosphere 2002: a comparison to Northern Hemisphere phenomena. *Journal of the Atmospheric Sciences*, *62*(3), 603–613. doi: 10.1175/jas-3316.1

Lorenz, D. J., & DeWeaver, E. T. (2007). Tropopause height and zonal wind response to global warming in the IPCC scenario integrations. *Journal of Geophysical Research Atmospheres*, *112*(10), 1–11. doi: 10.1029/2006JD008087

Martius, O., Polvani, L. M., & Davies, H. C. (2009). Blocking precursors to stratospheric sudden warming events. *Geophysical Research Letters*, *36*(14), 1–5. doi: 10.1029/2009GL038776

O'Neill, A., Oatley, C. L., Charlton-Perez, A. J., Mitchell, D. M., & Jung, T. (2017). Vortex splitting on a planetary scale in the stratosphere by cyclogenesis on a subplanetary scale in the troposphere. *Quarterly Journal of the Royal Meteorological Society*, *143*(703), 691–705. doi: 10.1002/qj.2957

Peings, Y. (2019). Ural blocking as a driver of early winter stratospheric warmings. *Geophysical Research Letters*, 2019GL082097. doi: 10.1029/2019GL082097

Quiroz, R. S. (1986). The association of stratospheric warmings with tropospheric blocking. *Journal of Geophysical Research*, *91*(D4), 5277. doi: 10.1029/jd091id04p05277

Saffin, L., Gray, S. L., Methven, J., & Williams, K. D. (2017). Processes maintaining tropopause sharpness in numerical models. *Journal of Geophysical Research: Atmospheres*, *122*(18), 9611–9627. doi: 10.1002/2017JD026879

Taguchi, M. (2014). Predictability of major stratospheric sudden warmings of the vortex split type: case study of the 2002 southern event and the 2009 and 1989 northern events. *Journal of the Atmospheric Sciences*, *71*(8), 2886–2904. doi: 10.1175/jas-d-13-078.1

Taguchi, M. (2018). Comparison of subseasonal-to-seasonal model forecasts for major stratospheric sudden warmings. *Journal of Geophysical Research: Atmospheres*, *123*(18), 10,231–10,247. doi: 10.1029/2018JD028755

Tamarin, T., & Kaspi, Y. (2017). The poleward shift of storm tracks under global warming: a Lagrangian perspective. *Geophysical Research Letters*, *44*(20), 10,666–10,674. doi: 10.1002/2017GL073633

Thompson, D. W., & Wallace, J. M. (2000). Annular modes in the extratropical circulation. Part I: month-to-month variability. *Journal of Climate*, *13*(5), 1000–

1016. doi: 10.1175/1520-0442(2000)013⟨1000:AMITEC⟩2.0.CO;2

Tripathi, O. P., Baldwin, M., Charlton-Perez, A., Charron, M., Cheung, J. C. H., Eckermann, S. D., . . . Stockdale, T. (2016). Examining the predictability of the stratospheric sudden warming of January 2013 using multiple NWP systems. *Monthly Weather Review*, *144*(5), 1935–1960. doi: 10.1175/MWR-D-15-0010.1

Tripathi, O. P., Baldwin, M., Charlton-Perez, A., Charron, M., Eckermann, S. D., Gerber, E., . . . Son, S. W. (2015). The predictability of the extratropical stratosphere on monthly time-scales and its impact on the skill of tropospheric forecasts. *Quarterly Journal of the Royal Meteorological Society*, *141*(689), 987–1003. doi: 10.1002/qj.2432

Vitart, F., Ardilouze, C., Bonet, A., Brookshaw, A., Chen, M., Codorean, C., . . . Zhang, L. (2017). The subseasonal to seasonal (S2S) prediction project database. *Bulletin of the American Meteorological Society*, *98*(1), 163–173. doi: 10.1175/BAMS-D-16-0017.1

White, I., Garfinkel, C. I., Gerber, E. P., Jucker, M., Aquila, V., & Oman, L. D. (2019). The downward influence of sudden stratospheric warmings: association with tropospheric precursors. *Journal of Climate*, *32*(1), 85–108. doi: 10.1175/JCLI-D-18-0053.1

514 **Table 1.**   Major SSWs in the period 1979–2017 (following Karpechko et al. (2017)) and the

515 peak value of the S-G dipole in the 15 days before the event according to ERA-Interim reanaly-

516 sis. Those events exceeding 40 hPa are shown in bold.

SSW event	Peak S-G index (hPa)
February 1979	**41**
February 1980	**43**
March 1981	**48**
December 1981	13
February 1984	**45**
January 1985	**44**
January 1987	**43**
December 1987	26
March 1988	21
February 1989	39
December 1998	34
February 1999	18
March 2000	24
February 2001	31
December 2001	24
January 2003	2
January 2004	12
January 2006	**42**
February 2007	17
February 2008	**40**
January 2009	22
February 2010	36
January 2013	27
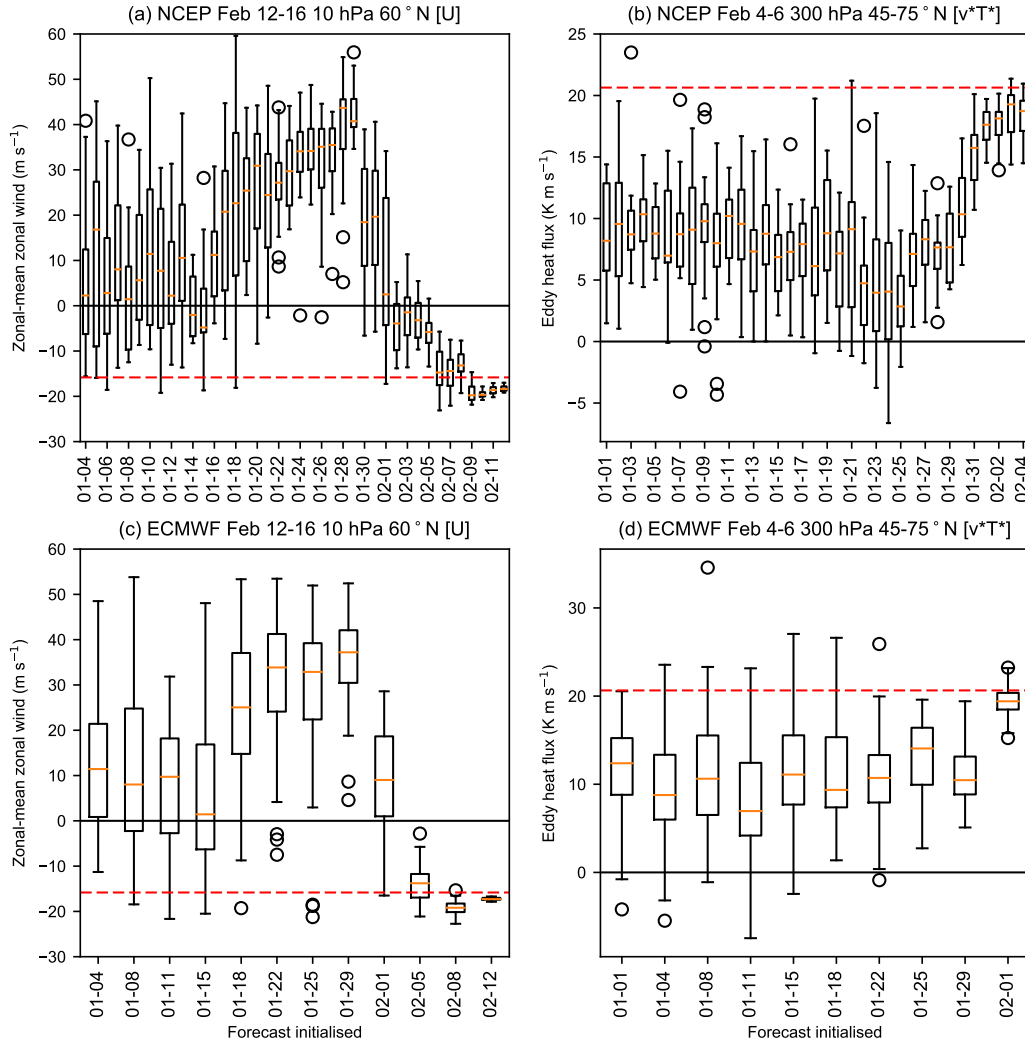
Figure 1. Boxplots showing (a), (c) average 10 hPa 60°N zonal-mean zonal-winds for 12–16 February 2018 and (b), (d) 300 hPa 45–75°N meridional eddy heat flux averaged over 4–6 February 2018 in (a), (b) NCEP and (c), (d) ECMWF models for all ensemble members as a function of initialisation date. Boxes indicate the interquartile range (IQR), whiskers extend to the last point less or greater than 1.5 times the IQR, with circles indicating outliers. The dashed red lines indicate verifying values according to ERA-Interim reanalysis.
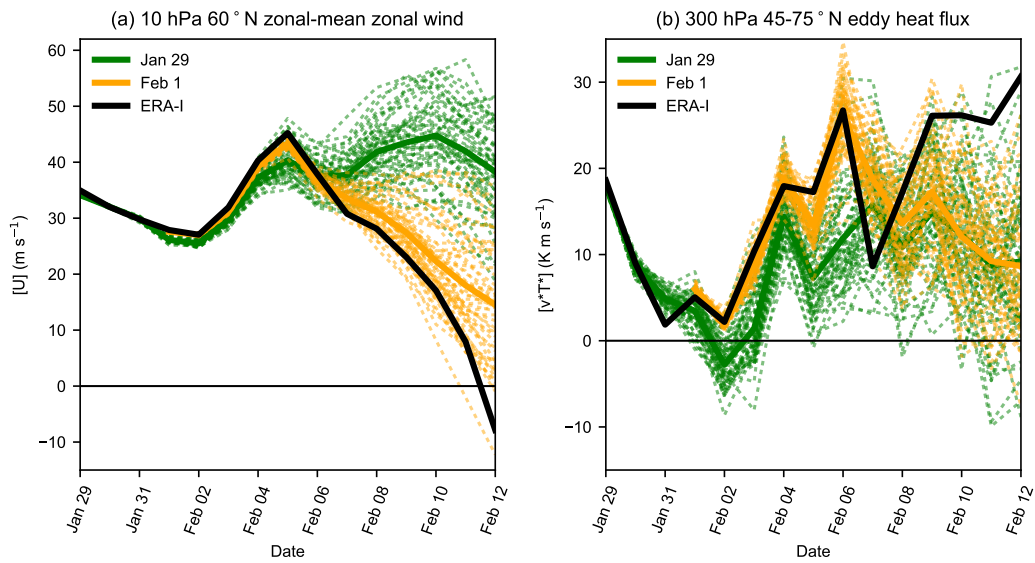
Figure 2. ECMWF ensemble forecasts from 29 January (dashed green) and 1 February

(dashed orange) for (a) 10 hPa 60°N zonal-mean zonal wind and (b) 300 hPa 45–75°N meridional

eddy heat flux for 29 January–12 February 2018. Ensemble means are shown with thick lines.

Verifying evolution from ERA-Interim is shown with the thick black line.
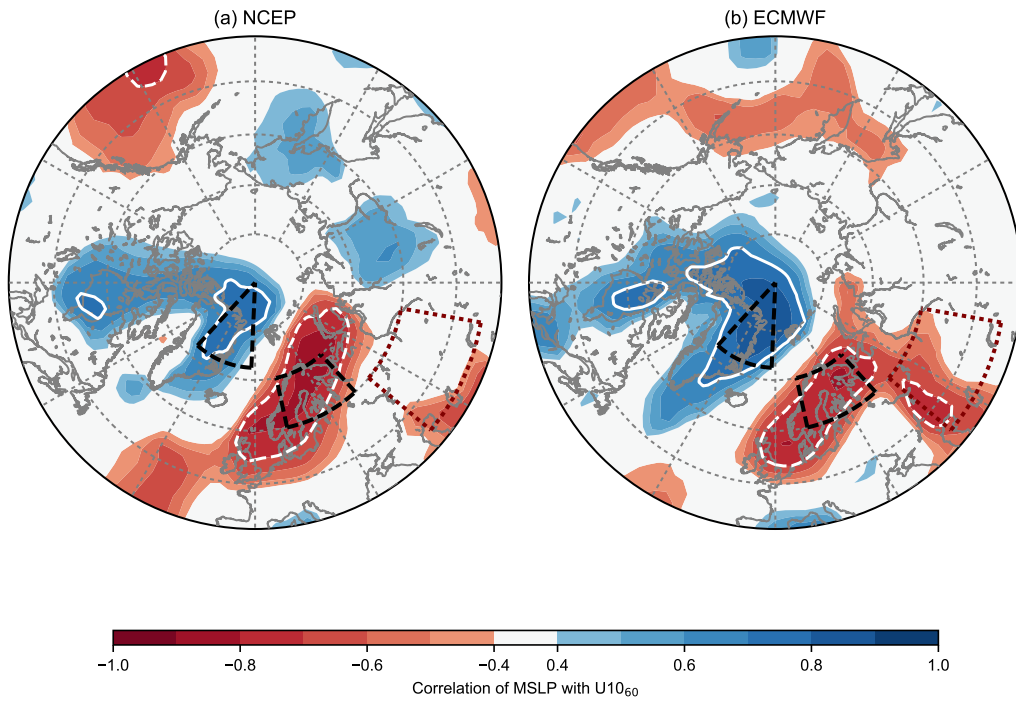
Figure 3. Linear correlation between average 9–11 February $U10_{60}$ and average 3–5 February mean MSLP from (a) 29 January to 1 February NCEP forecasts and (b) 29 January and 1 February ECMWF forecasts. White lines delineate where the magnitude of the correlation exceeds 0.7. The two nodes of the S-G dipole are shown with black dashed lines, and the location of the Ural high is shown with maroon dotted lines.
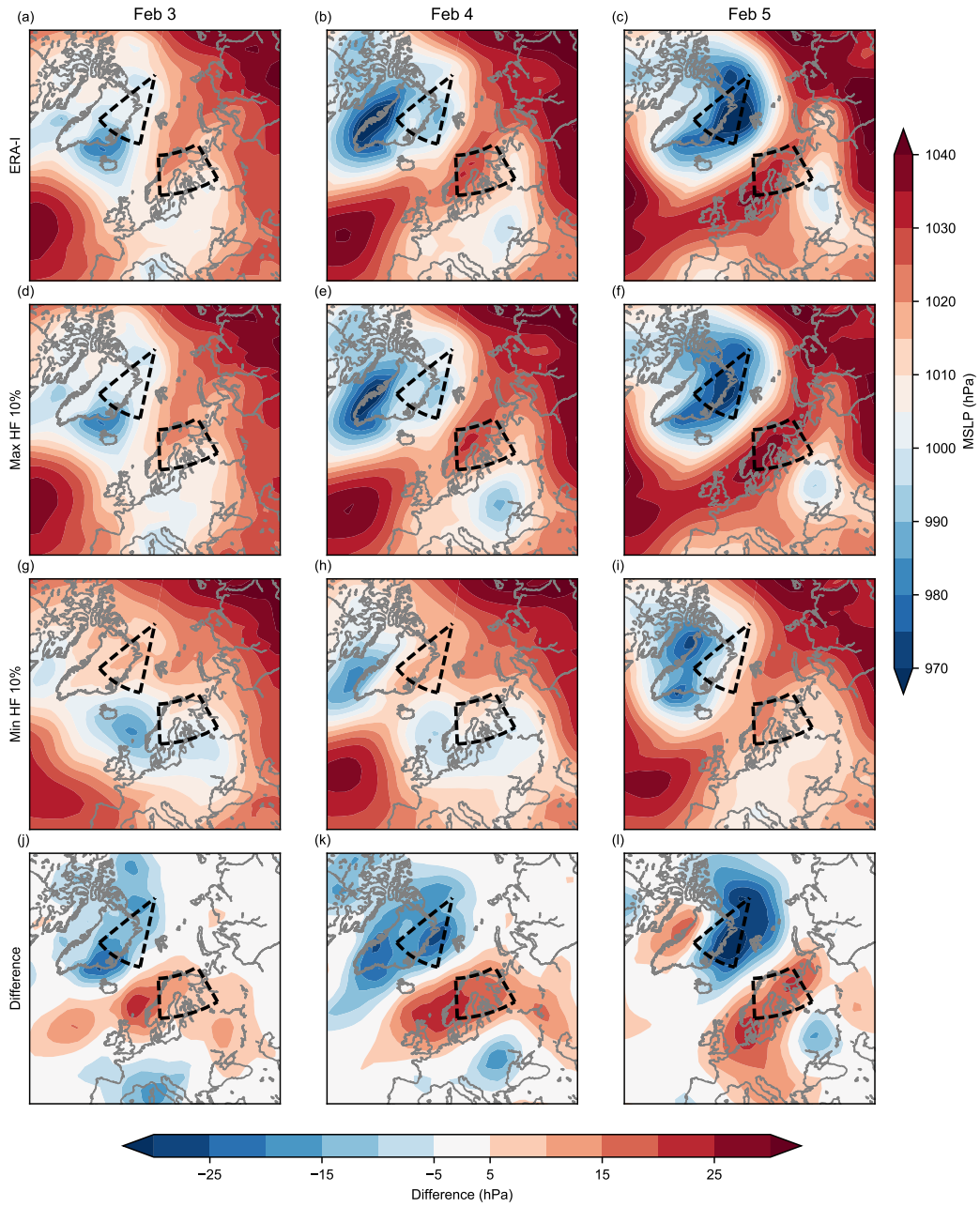
Figure 4. MSLP for 3–5 February from (a-c) ERA-Interim reanalysis, (d-f) the mean forecast from members of the ECMWF 29 January and 1 February joined ensemble with the top 10% 300 hPa 45–75°N heat flux on 4–6 February, (g-i) the bottom 10%, and (j-l) the difference (d-f – g-i). The two nodes of the S-G dipole are shown with black dashed lines.
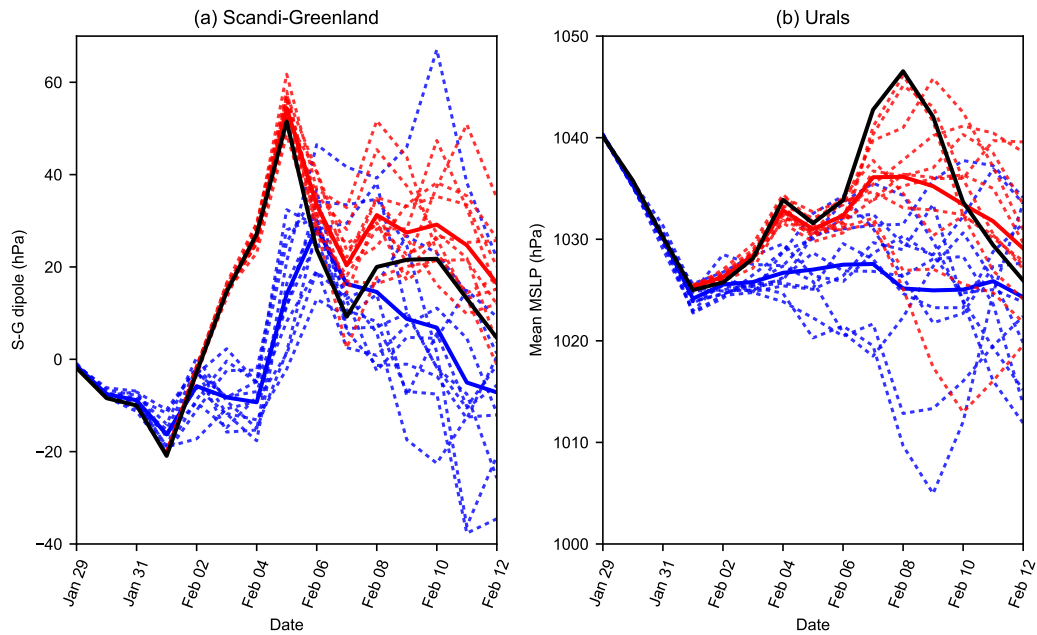
Figure 5. Time series of ECMWF ensemble forecasts from 29 January 1 February for (a) the S-G dipole and (b) the Ural high from members with the top (dotted red) and bottom (dotted blue) 10% mean 4–6 February 300 hPa 45–75°N [v*T*]. Their respective means are shown with thick lines coloured accordingly. The verifying evolution from ERA-Interim is shown in black.
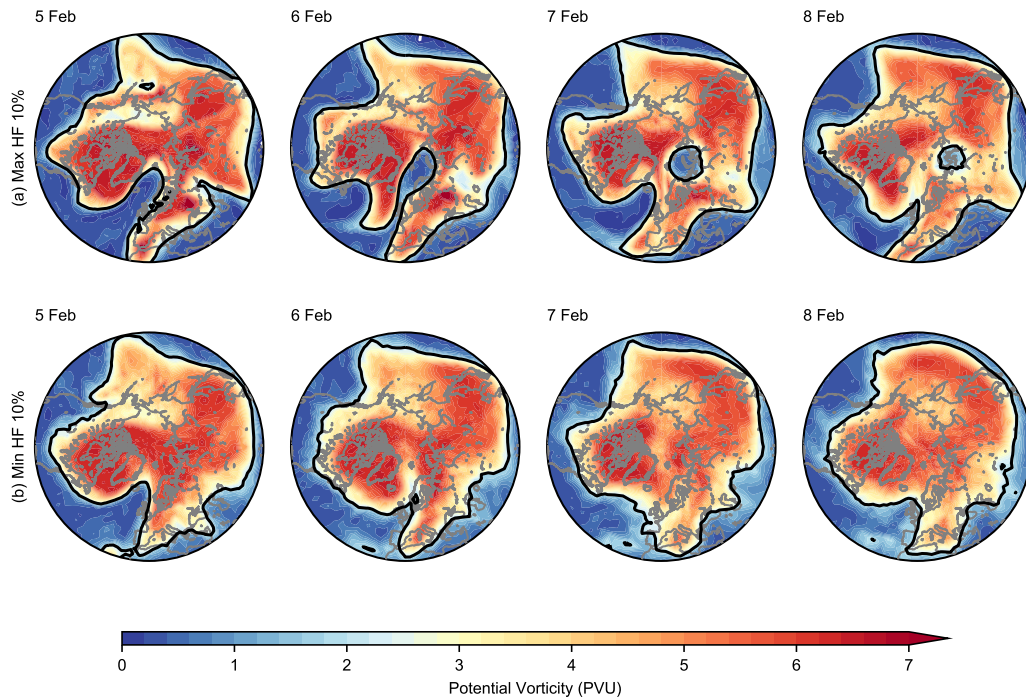
Figure 6. Forecasts of PV on the 320 K isentropic surface for 5–8 February from members of the ECMWF 29 January and 1 February joined ensemble. (a) shows the mean forecast from members with the top 10% 300 hPa 45–75°N heat flux on 4–6 February and (b) the bottom 10%. The 2 PV unit isoline (PVU, where 1 PVU = 10^{-6} m^2 s^{-1} K kg^{-1}) is contoured in black.
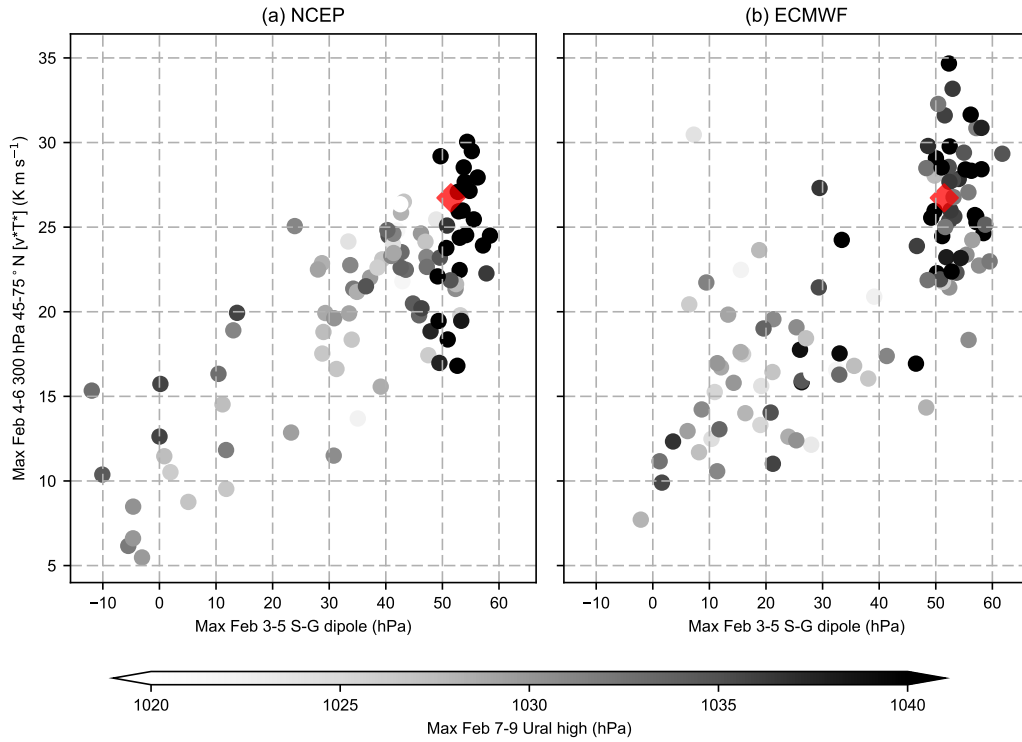
Figure 7. Scatter plots of maximum 4–6 February 300 hPa [v*T*] versus maximum 3–5 February mean S-G dipole for (a) NCEP ensembles from 29 January to 3 February ($n = 96$), and (b) ECMWF ensembles from 29 January and 1 February ($n = 102$). The points are coloured by the corresponding maximum 7–9 February Ural high strength. The verifying ERA-Interim value is shown with a red diamond.
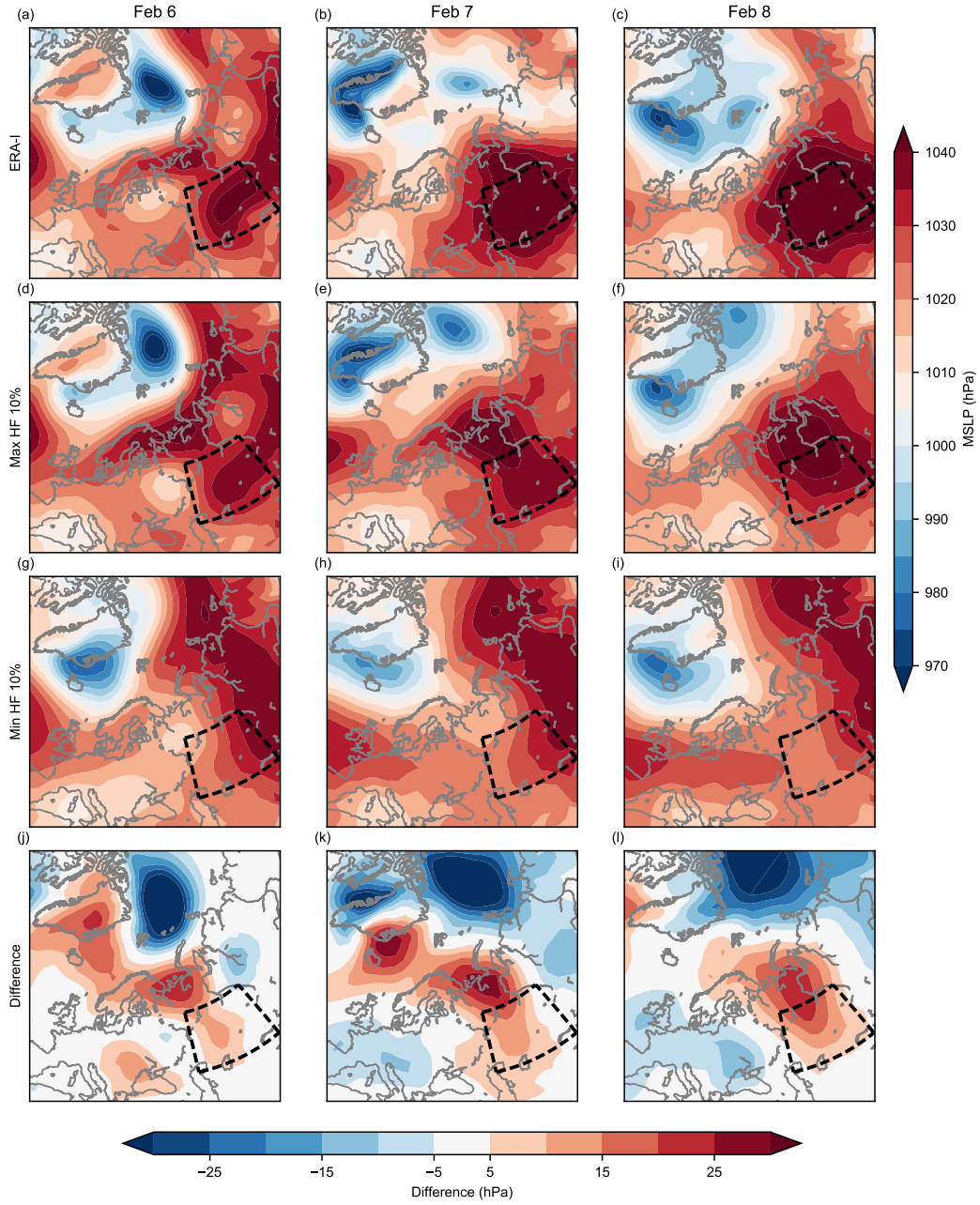
Figure 8. As in Figure 4 but for 6–8 February. The Ural high is indicated with black dashed lines.

–27–
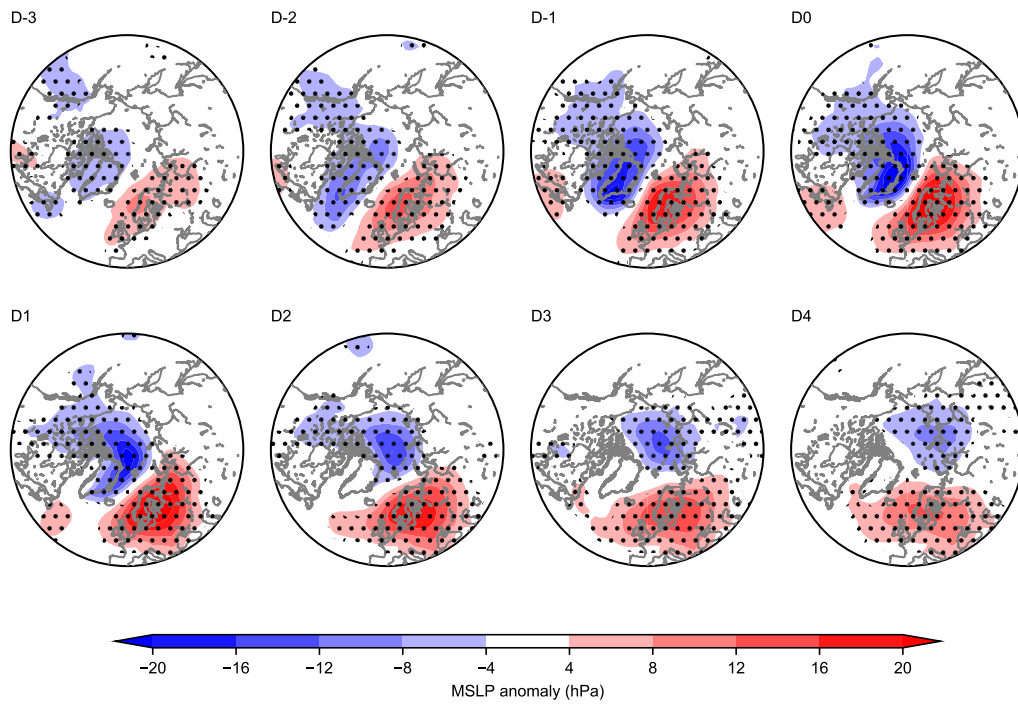
Figure 9. Composite of MSLP anomalies (with respect to January 1979–March 2017 climatology) from ERA-Interim for the period 3 days before to 4 days after 49 historical S-G dipole events exceeding 40 hPa. Stippling indicates areas significant at the 95% confidence level (for details see Section 2).
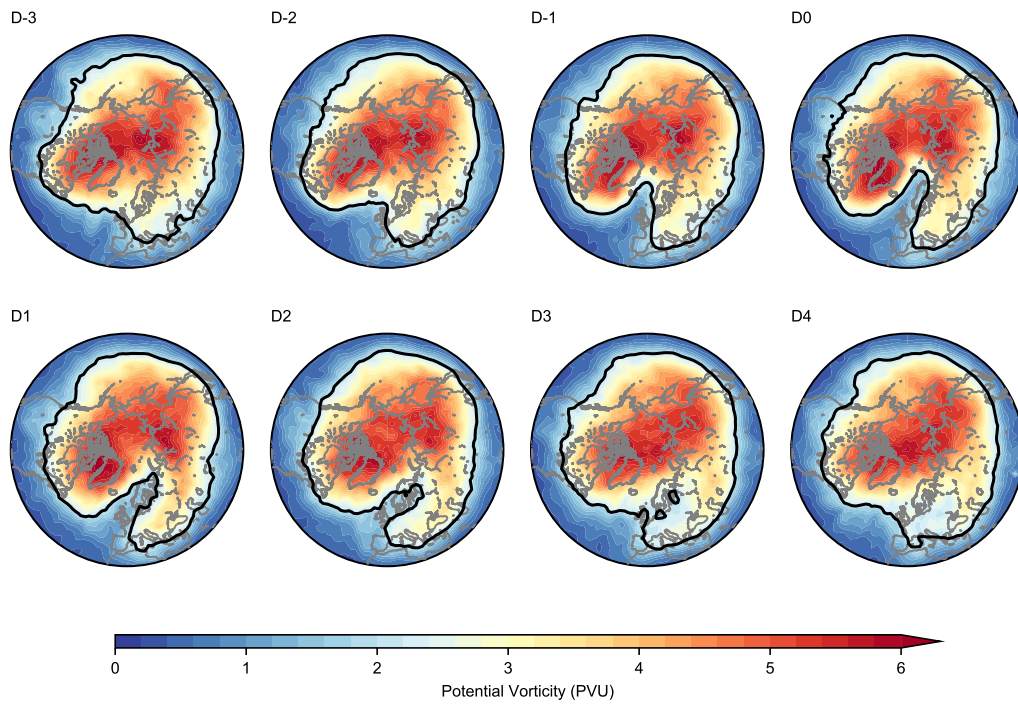
Figure 10. As in Figure 9 but for PV on the 315 K isentropic surface. The thick black line indicates the 2 PVU contour.
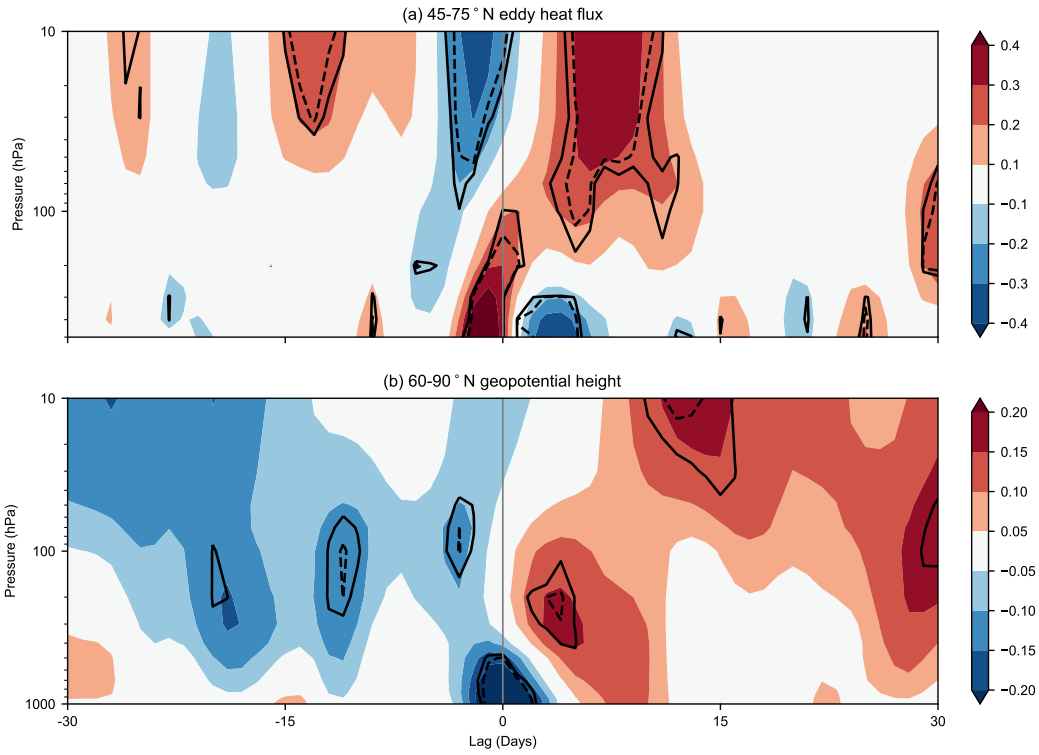
Figure 11. Composite of anomalies in (a) 45–75°N meridional eddy heat flux [v*T*] and (b) 60–90°N geopotential height for 30 days before and after 49 events in ERA-Interim 1979–2017 where the S-G dipole exceeded 40 hPa. Anomalies are standardized departures and are filtered using a 1 σ Gaussian smoother; in (b) these are shown relative to the mean for the 61-day window to show relative tendency. The gray vertical line indicates the day on which the 40 hPa threshold was exceeded. Solid (dashed) black contours indicate regions significant at the 90% (95%) confidence level (for details see Section 2).

Figure 1.

(a) NCEP Feb 12-16 10 hPa 60 ° N [U]
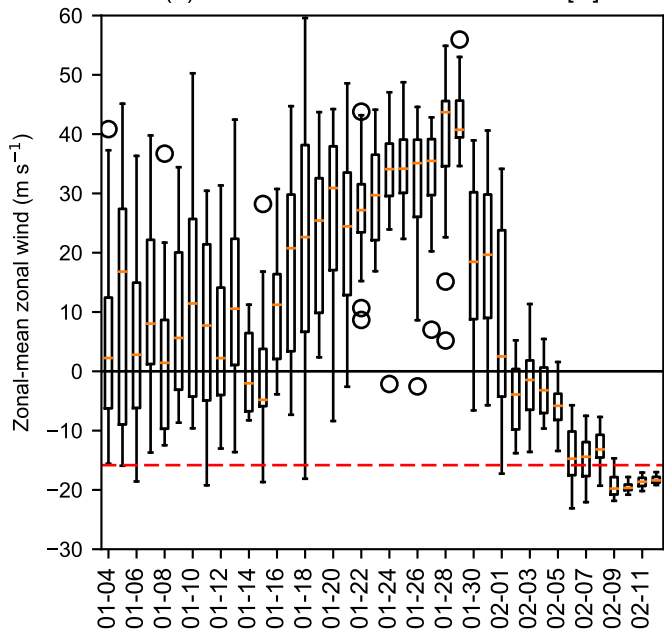
(b) NCEP Feb 4-6 300 hPa 45-75 ° N [v*T*]
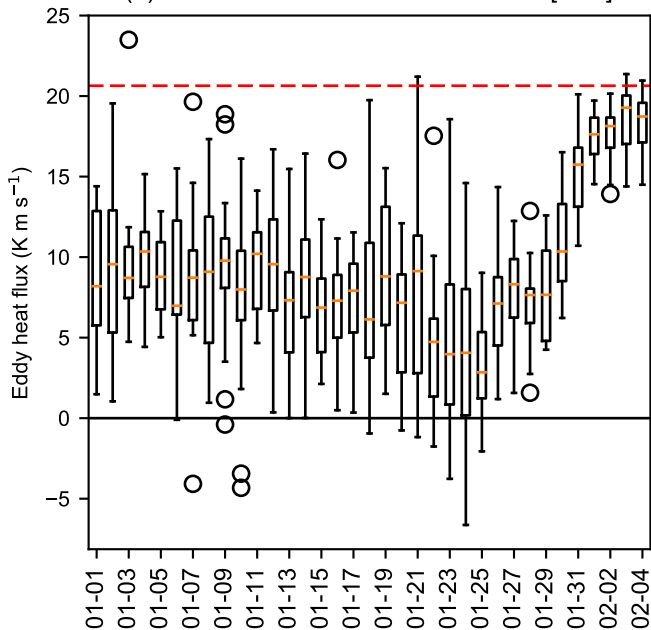
(c) ECMWF Feb 12-16 10 hPa 60 ° N [U]
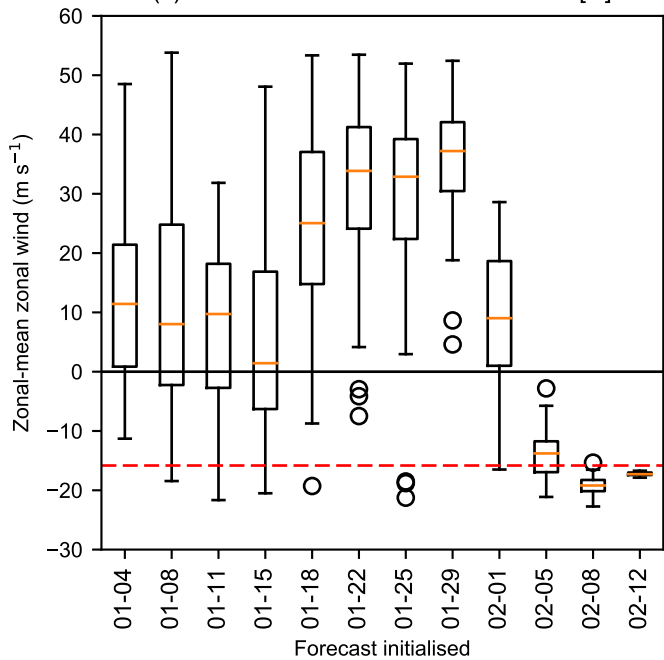
(d) ECMWF Feb 4-6 300 hPa 45-75 ° N [v*T*]
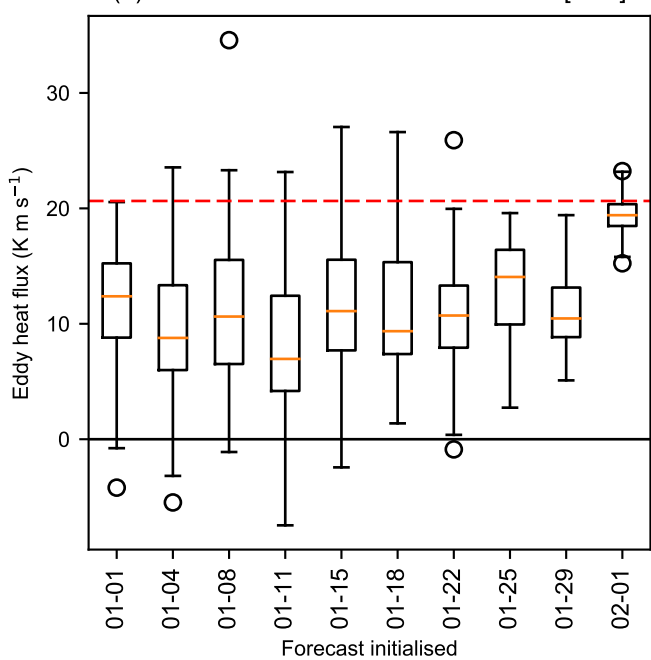
Figure 2.

(a) 10 hPa 60°N zonal-mean zonal wind
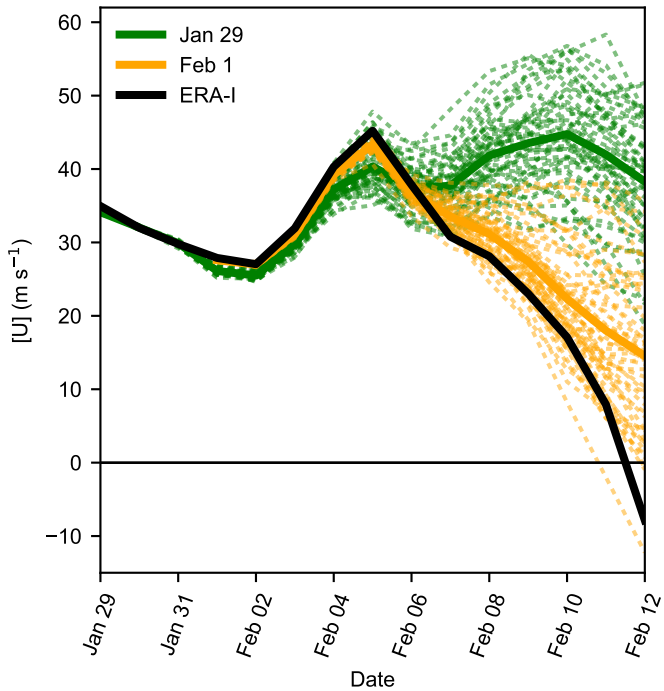
(b) 300 hPa 45-75°N eddy heat flux

Figure 3.

(a) NCEP   (b) ECMWF

Correlation of MSLP with $U10_{60}$
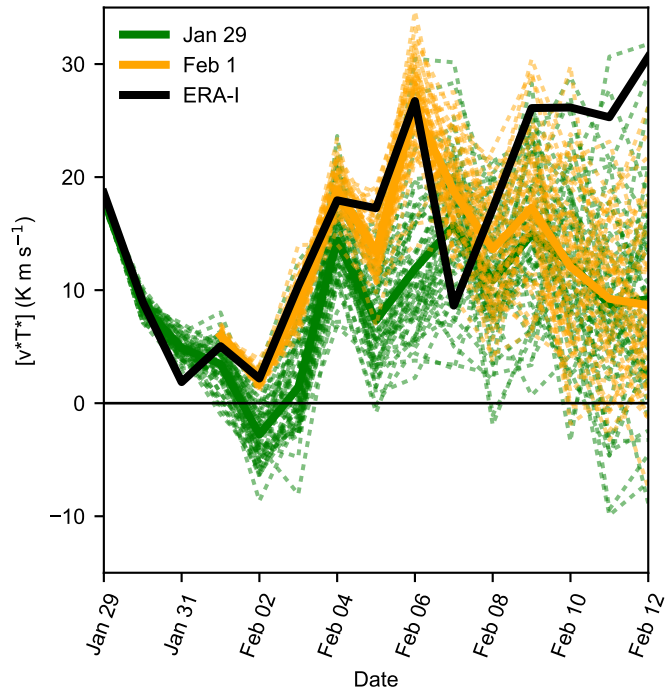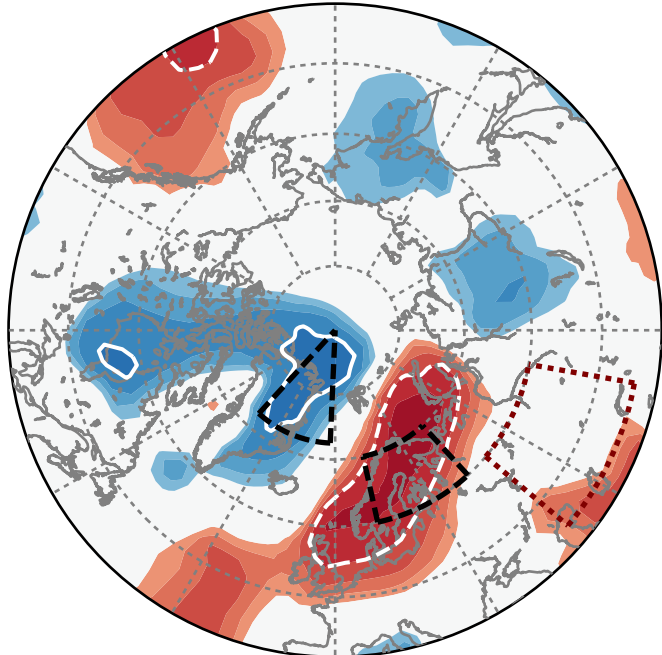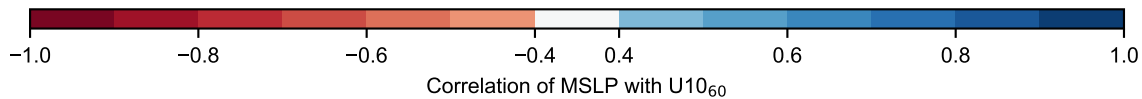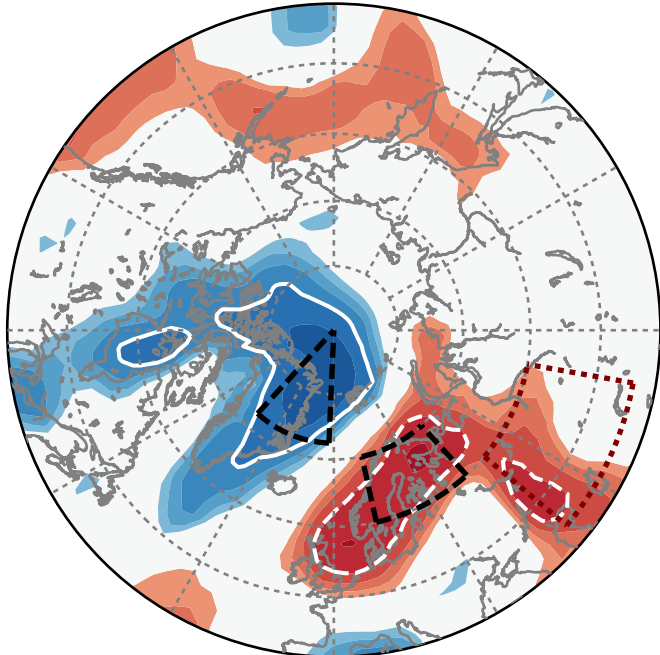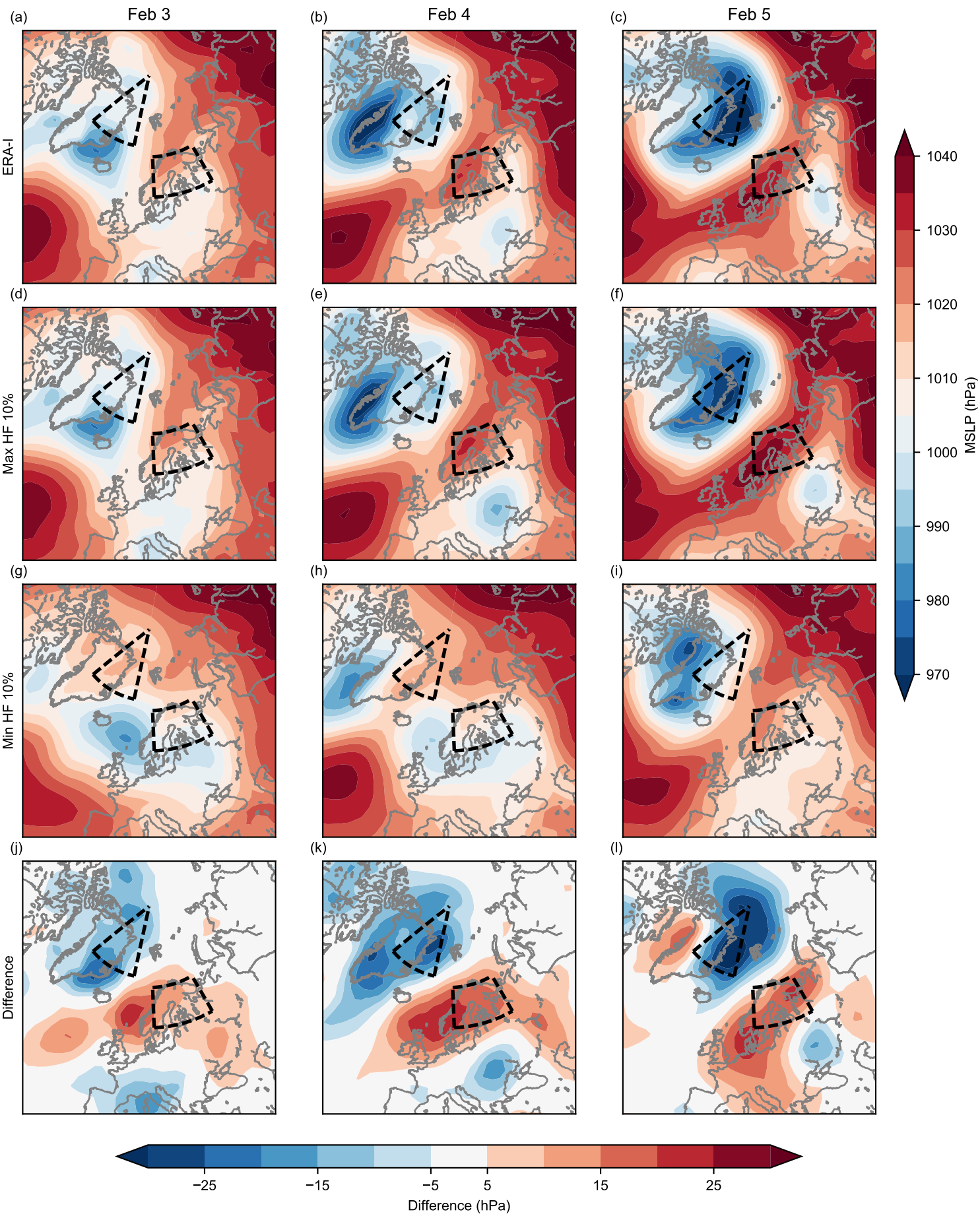
Figure 4.

Figure 5.

(a) Scandi-Greenland
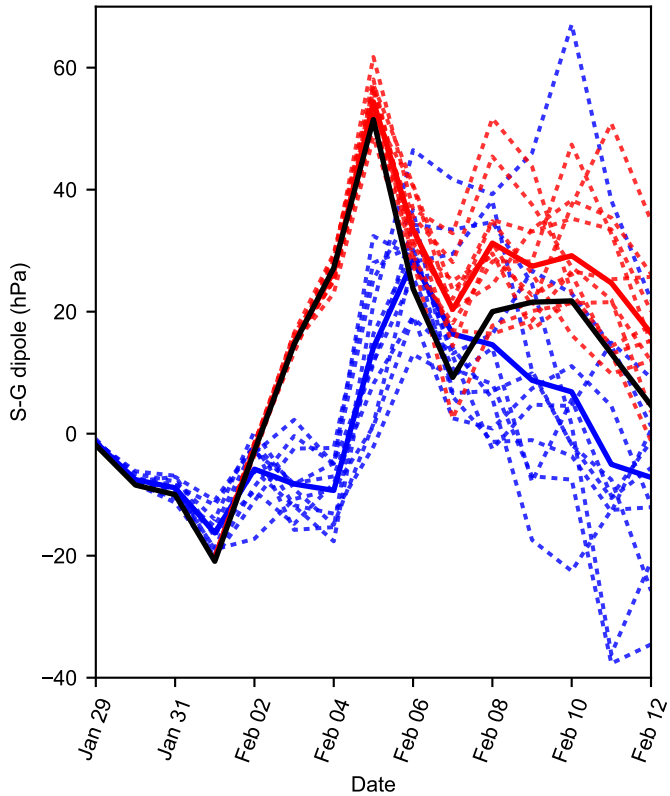
(b) Urals
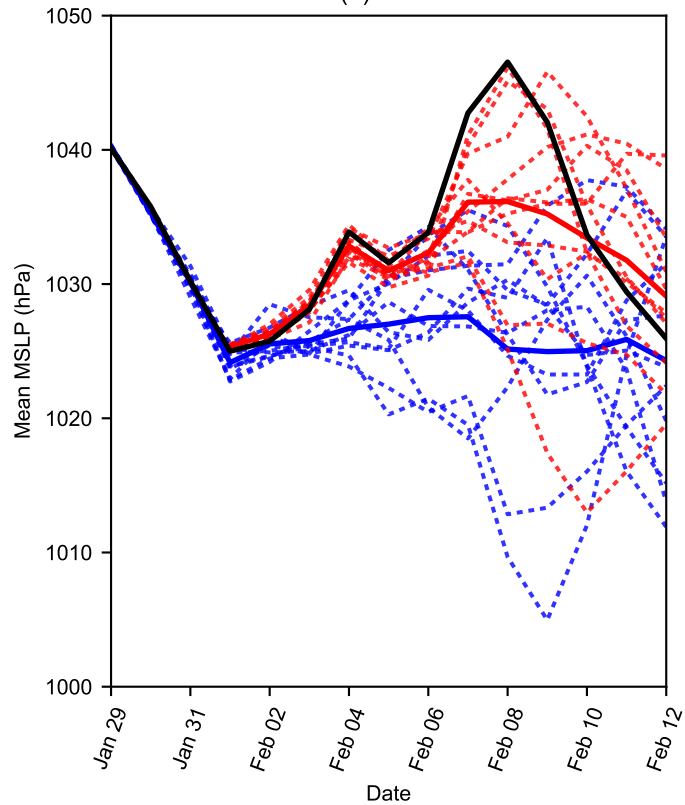
Figure 6.
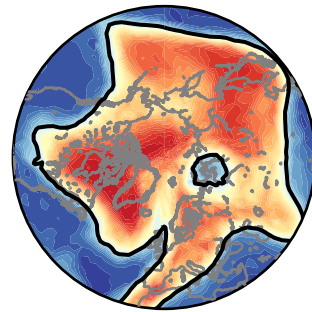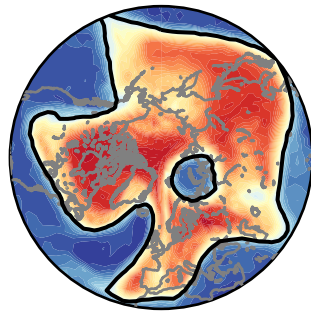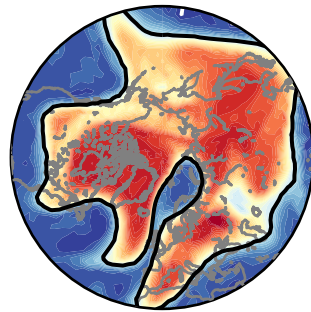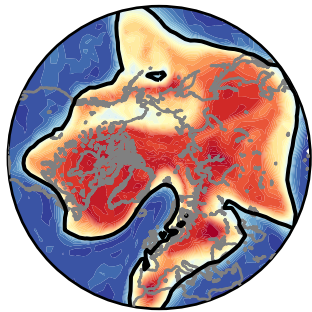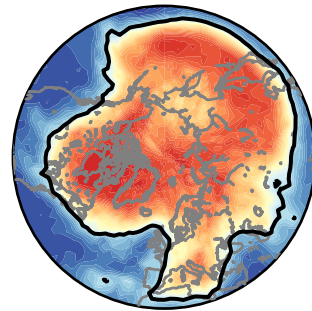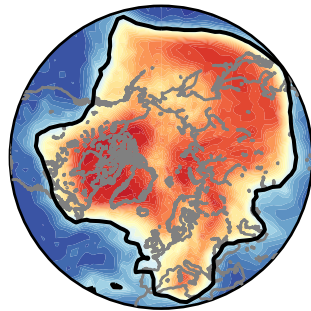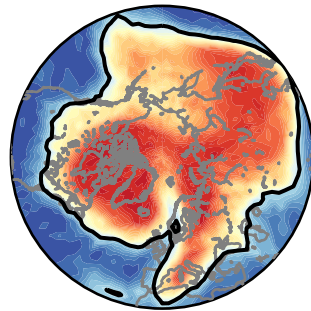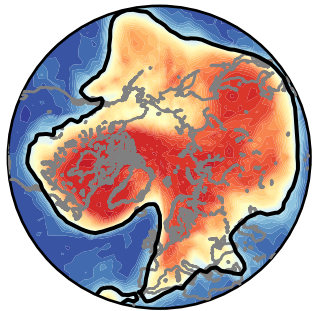
Potential Vorticity (PVU)

Figure 7.

Figure caption area:

(a) NCEP

(b) ECMWF

Max Feb 3-5 S-G dipole (hPa)

Max Feb 4-6 300 hPa 45-75° N [v*T*] (K m s^{-1})

Max Feb 7-9 Ural high (hPa)

Figure 8.

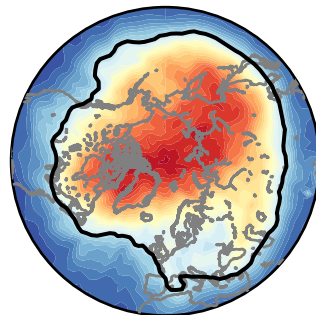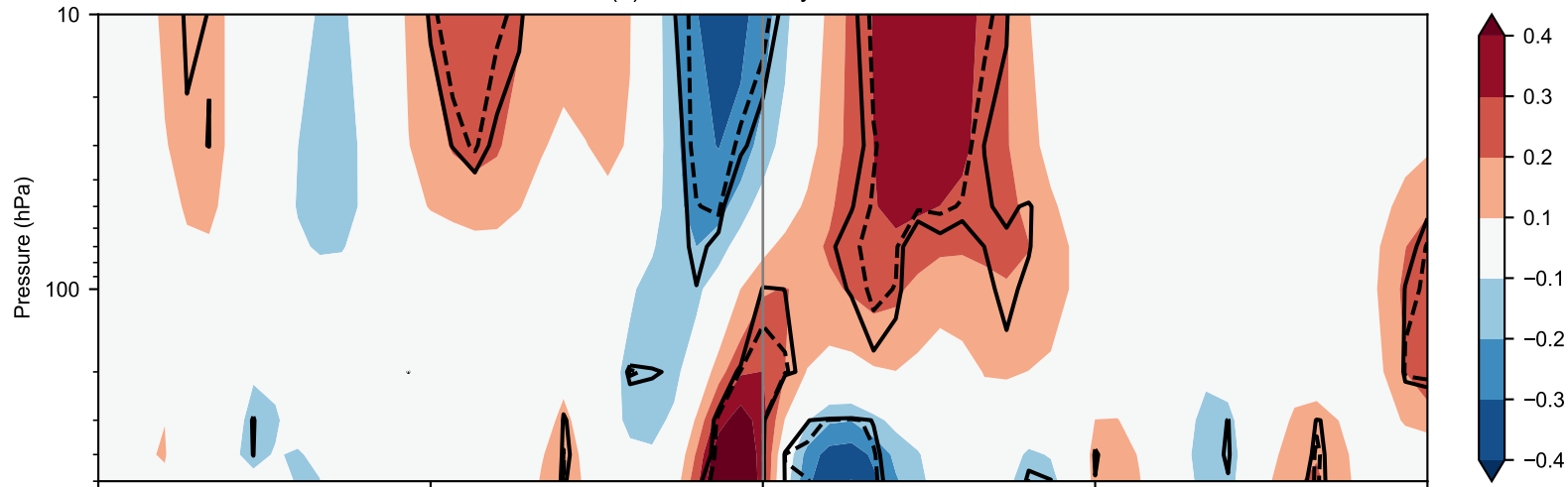**Figure 9.**

MSLP anomaly (hPa)
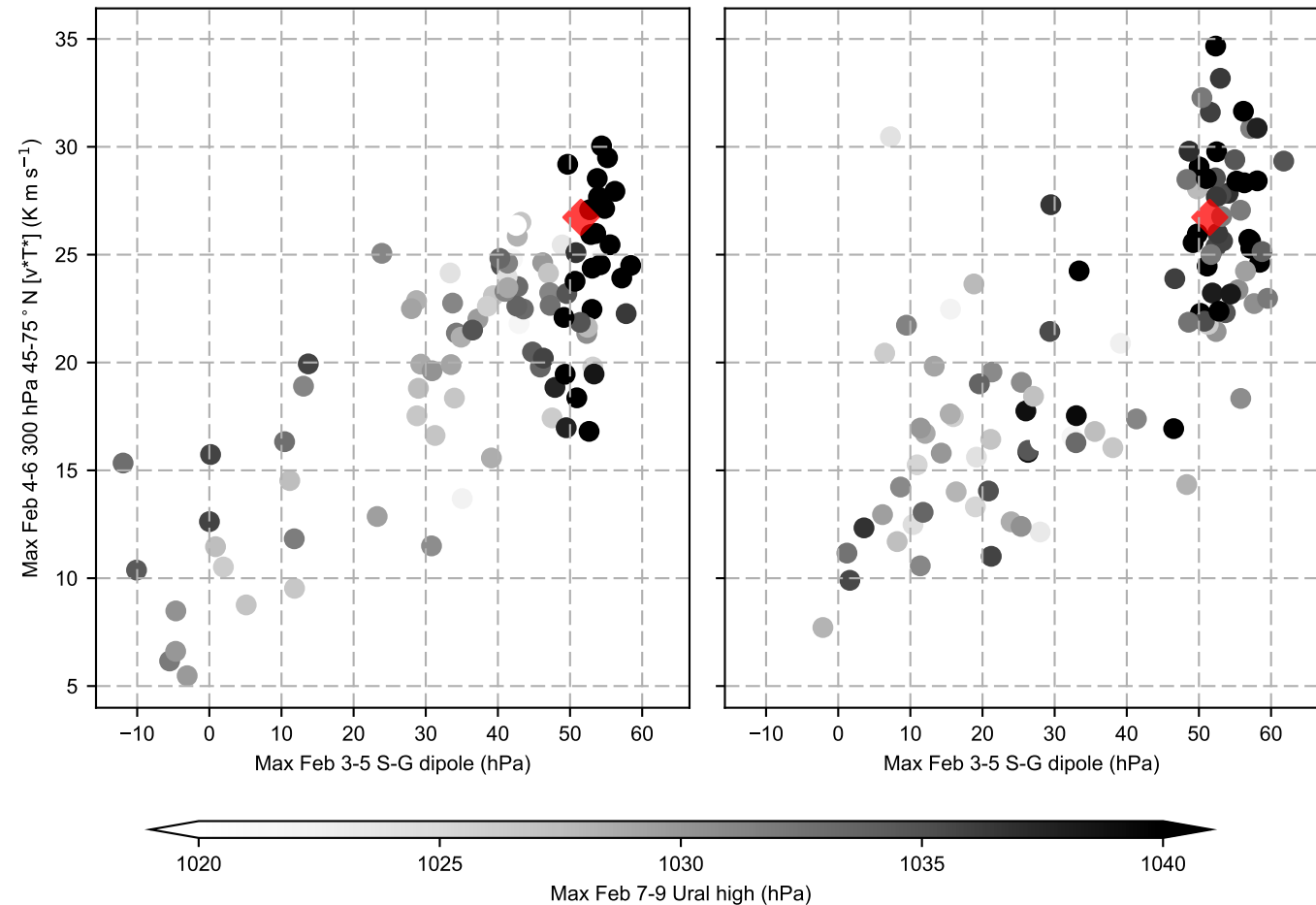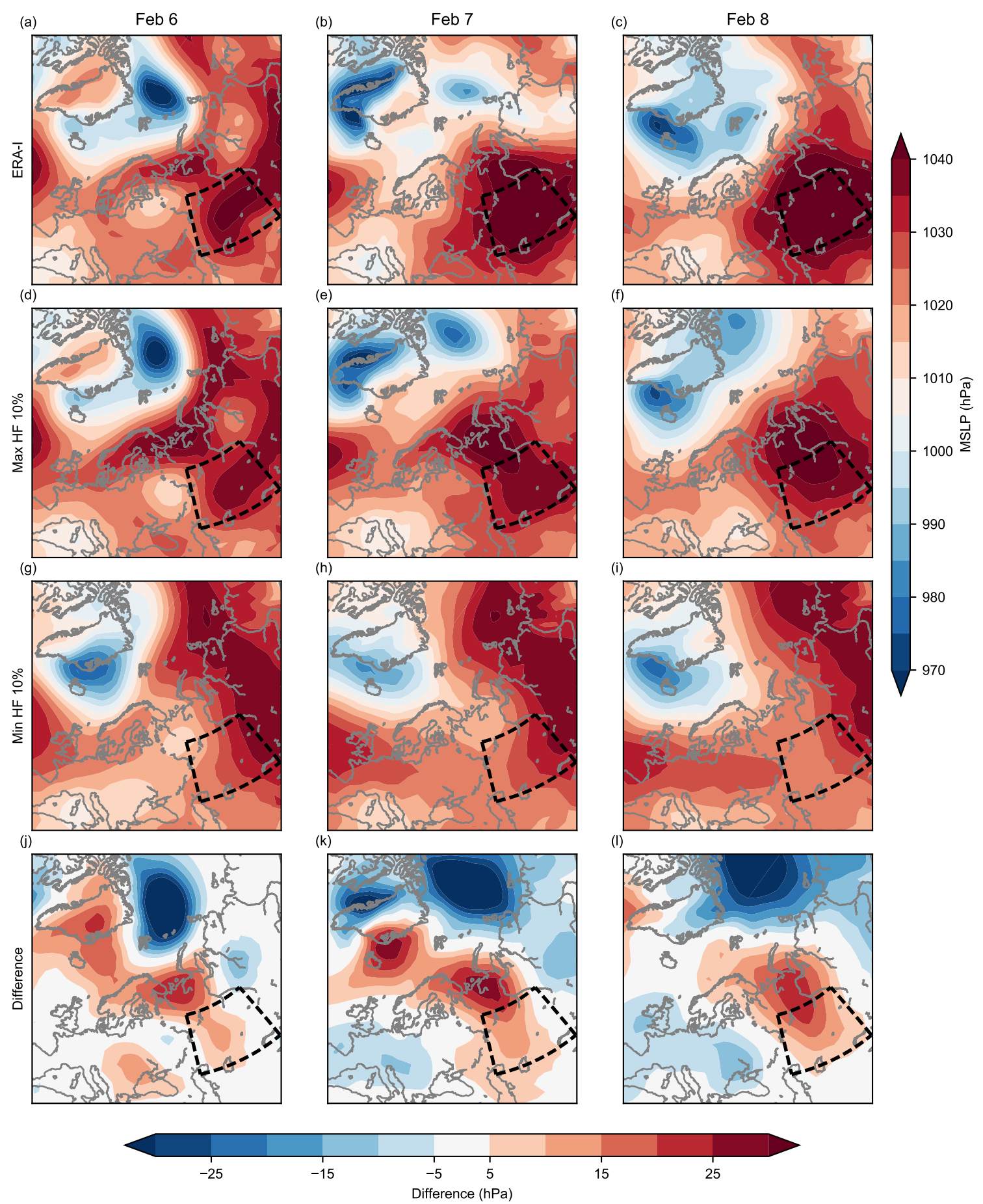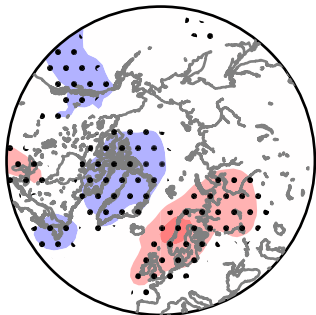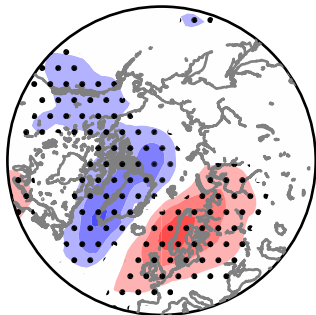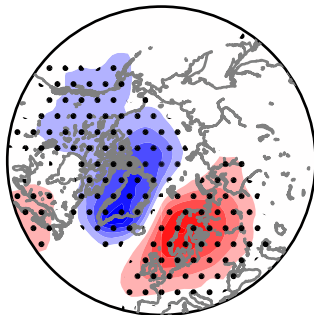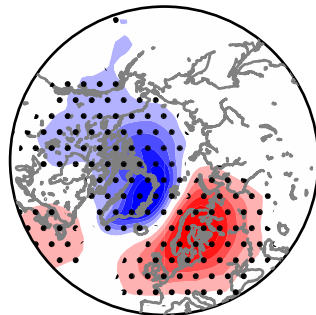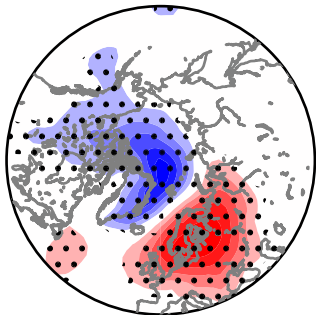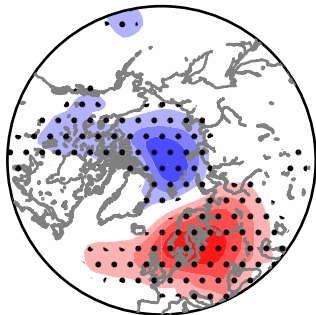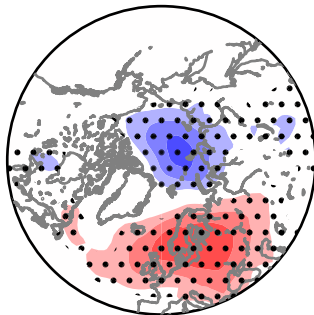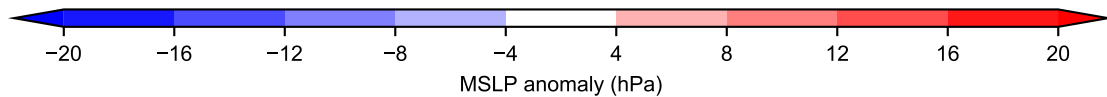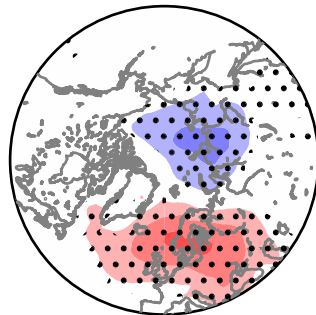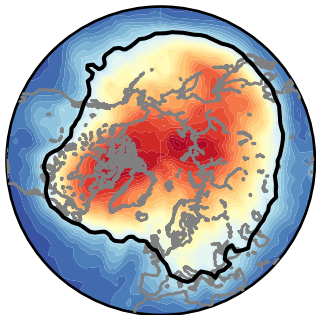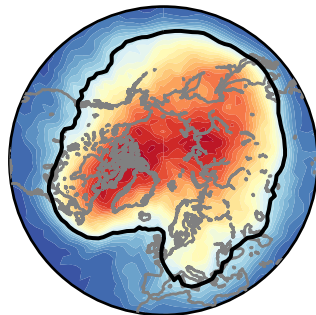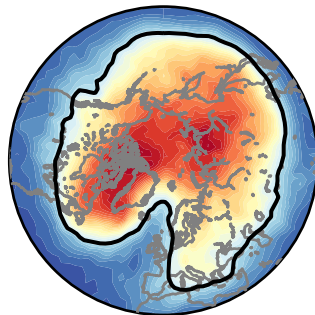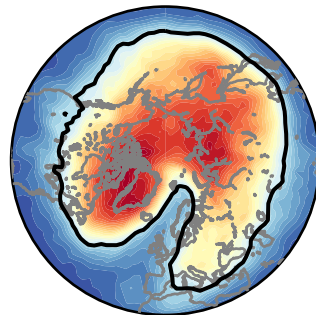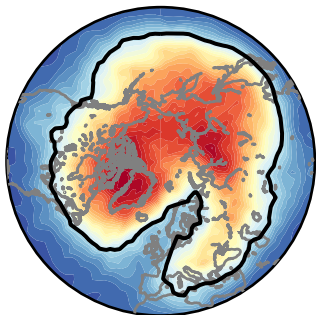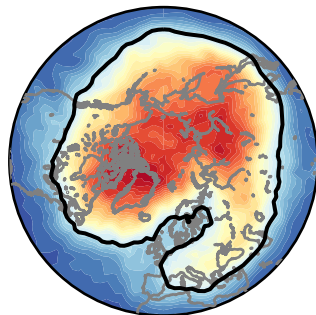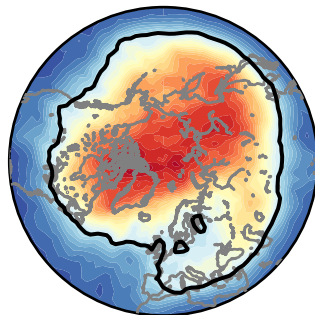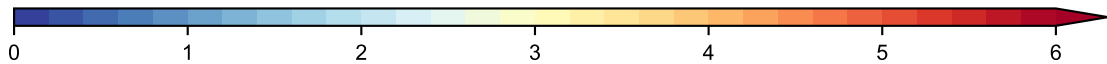
Figure 10.

Potential Vorticity (PVU)

Figure 11.

(a) 45-75 ° N eddy heat flux

(b) 60-90 ° N geopotential height